National University of Science and Technology POLITEHNICA Bucharest

Doctoral School of Power Engineering

Ph.D. Thesis Summary:

Creșterea eficienței energetice a suflantelor centrifugale prin dezvoltarea unui sistem integrat de reglare continuă a debitului

Increasing the Energetic Efficiency of Centrifugal Blowers by Development of an Integrated Continuous Flow Control System

Author: CS. III ing. Teodor STĂNESCU

Ph.D. Evaluation Board:

Chairman	Prof.dr.ing. Radu PORUMB	UNST POLITEHNICA Bucharest
Ph.D. supervisor	**Prof.em.dr.ing. Dan Niculae ROBESCU**	UNST POLITEHNICA Bucharest
Referent	CS. I. dr.ing. Gheorghe FETEA	INCDT COMOTI
Referent	Prof.dr.ing. Diana Maria BUCUR	UNST POLITEHNICA Bucharest
Referent	Prof.dr.ing. Ilare BORDEAȘU	POLITEHNICA University Timisoara

BUCHAREST

2020 – 2024

Table of Contents

Notation and Symbols

Latin and Greek Letters

b	Blade width	S	Blade thickness
c	Absolute velocity	SST	Shear Stress Transport
c_m	Flow velocity	t	Temperature expressed in °C
c_u	Tangential velocity	T	Temperature expressed in K
CFD	Computational Fluid Dynamics	u	Blade velocity
D	Diameter	v	Absolute velocity
FDM	Fused Deposition Modeling	VVD	Variable Vane Diffuser
H	Head	w	Relative velocity
I	Electric current intensity	y	Wall-normal coordinate
IGV	Inlet Guide Vane	z	Number of blades
k	Turbulent kinetic energy	α	Absolute angle at inlet/outlet
L	Total length	β	Angle to the impeller blade
$\dot{m}$	Mass flow rate	ε	Error
n	Rotation speed	η	Efficiency
p	Pressure	π_c	Pressure ratio
P	Power	ω	Angular velocity; Specific rate of dissipation
Q	Volumetric flow rate		

Superscripts

`	lower flow rates than the nominal one	``	higher flow rates than the nominal one

Subscripts

0	Reference state; Impeller inlet; Initial moment	d	Dynamics
		g	Gas dynamics
1	Initial state; Impeller blade inlet	m_{H2O}	Expressed in meters water column
2	Impeller outlet; Final state	s	Static
3	IGV inlet	SJ	Spherical joints
4	SPR outlet; Volute inlet	t	Total
5	Volute outlet; Discharge section		

Conventions

- bara absolute pressure expressed in bar (relative to *p* = 0);
- barg relative pressure (the difference between absolute pressure and the reference pressure) expressed in bar.

Keywords: energy efficiency, turbomachinery, inlet guide vane, variable vane diffuser, CFD analysis, centrifugal blower.

INTRODUCTION

The first centrifugal blower models were developed and produced on an industrial scale at the start of the 20th century. These machines maintain a steady pressure at the discharge flange and distinguish themselves from volumetric blowers by how they convert mechanical energy from the motor into gas pressure energy. This conversion process primarily involves turning the mechanical energy into kinetic energy through the centrifugal impeller. Then, with the help of the vane diffuser and volute, this kinetic energy is almost entirely transformed into pressure energy. Centrifugal blowers frequently intake air at atmospheric pressure. Various factors, such as the size or shape of aerodynamic components, the speed of the centrifugal impeller, the temperature of the gas being drawn in and pressure losses within the turbomachinery, can influence changes in operating parameters like flow or pressure. Decreasing all losses within the blowers consistently leads to improved operating efficiency.

Primarily, with the widespread introduction of numerical simulation programs based on the Navier-Stokes flow equations, the majority of specialized studies have focused on maximizing the optimization of aerodynamic components used in the construction of centrifugal blowers and compressors (such as the IGV, VVD, impeller, volute etc.) at their nominal operating points. In practice, due to the flow parameter, which needs adjustment in certain applications, the efficiency of the machines tends to decrease significantly over time. One solution that allows for maintaining these efficiencies at the highest values is to find an efficient method of flow control without altering the discharge pressure value. On one hand, if the pressure value decreases, the new value will often be incompatible with the application in which the turbomachine operates; and on the other hand, if the discharge pressure value increases, the total compression power also increases, leading to a much lower efficiency of the entire application.

In air compression applications, centrifugal blowers will always be present, especially in applications that aid in wastewater treatment. In treatment plants, air compression units must operate continuously for several years in a row, with the only acceptable stoppages being controlled ones for preventive maintenance, which are usually carried out quickly, within a few hours. Considering that in treatment plants the flow of wastewater entering the treatment processes varies from minute to minute, the machines that supply compressed air to the tanks must ensure the delivery of a variable amount of air at the highest possible efficiency, while maintaining constant working pressure.

The main objectives of the following thesis were based on the following points and requirements:

- Replacing the old centrifugal blowers used in wastewater treatment plants by designing and developing new ones that offer higher efficiencies in most stable operating points;

- Expanding the operating range of classic blowers by using variable inlet guide vanes and a variable vane diffuser;
- Developing a calculation methodology to assist in the preliminary sizing and design of centrifugal blowers;
- Finding a correlation law between those two stators (inlet guide vane and variable vane diffuser) so that when the mass flow rate changes, the working pressure remains constant without changing the operating speed, while also maintaining the highest efficiency levels;
- Designing mechanical control systems for the angular regulation of blades for these stators, specifically an independent control system where the IGV or VVD are operated separately, as well as an integrated system using a single actuator to control both stator blades;
- Designing and fabricating a scale model of a turbo blower to confirm the utility of new manufacturing methods for components, specifically additive manufacturing (using FDM-type 3D printers). These methods aim to generate models and prototypes of various objects, aiding in visualizing the components comprehensively and in detail, while also validating the designed mechanical system.

CHAPTER 1 The current stage of technical achievements and research in the field of blowers

Centrifugal blowers are pneumatic machines that ensure the circulation and compression of gases, being used in various applications, including wastewater treatment, dust removal, water aeration and so on.

Centrifugal blowers are primarily constructed of the following components:

- **Bellmouth**, located upstream of the impeller, assists in smoothing the fluid flow as it enters the turbomachinery;
- **Inlet guide vane**, comprising aerodynamically profiled blades, evenly spaced along a predetermined diameter, with the purpose of regulating the flow by modifying the tangential velocity component at the impeller inlet (c_{u1}). This effect is achieved by adjusting the angles of deployment of the IGV blades;
- **Centrifugal impeller**. It receives mechanical energy from the electric motor and transforms it into pneumatic energy (kinetic and pressure) through the blades;
- **Variable vane diffuser**, comprising aerodynamically profiled blades. It is responsible for converting a portion of the kinetic energy resulting from the impeller exit into pressure energy, primarily achieved by redirecting the gas flow;
- **Volute**. By increasing the flow section, it ensures the capture of flow from the impeller periphery (thus achieving speed field braking), thereby converting kinetic energy into pressure energy.

Apart from the mentioned aerodynamic components, centrifugal blowers may also incorporate additional units, such as: speed multiplier, oil pump (for lubrication system), intermediate couplings (e.g. between the electric motor and speed multiplier), oil tank, control panel and control unit. Figure 1.1 presents a type of centrifugal blower that contains all the elements presented earlier.

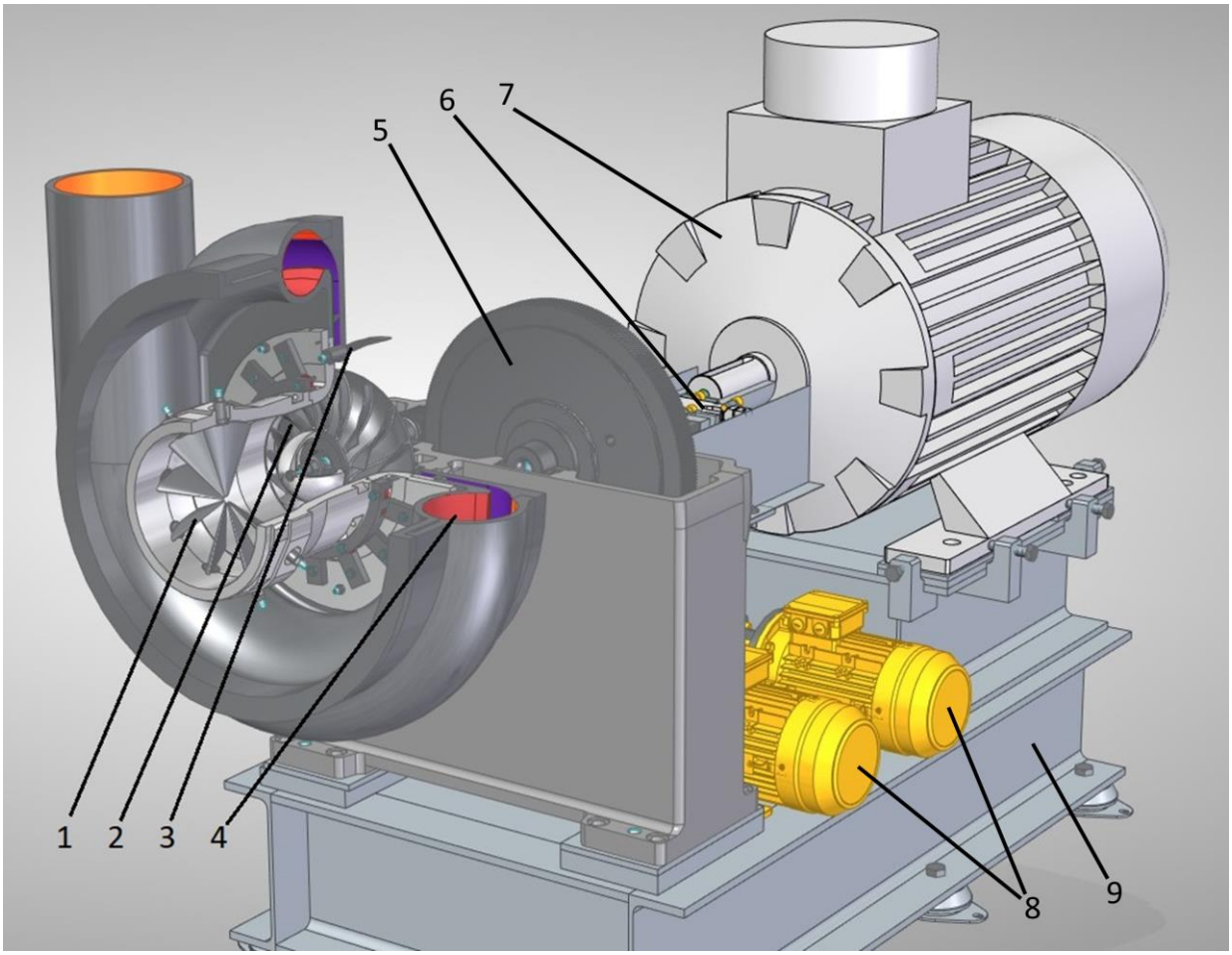

Fig. 1.1 Centrifugal blower assembly, where: 1 – inlet guide vane; 2 – centrifugal impeller; 3 – variable vane diffuser; 4 – volute; 5 – spur gear wheel of the speed multiplier; 6 – intermediate coupling; 7 – main electric motor; 8 – oil pump motors; 9 – base frame [image generated by the author]

The current chapter presents a synthesis of the most important articles and scientific works in the field of compressors and centrifugal blowers. This part of the work offers a comprehensive perspective on aerodynamic components and discusses ways to enhance the operational efficiency of turbomachinery.

1.1. Correlation Between VVD Blade Angle and IGV Blade Angle

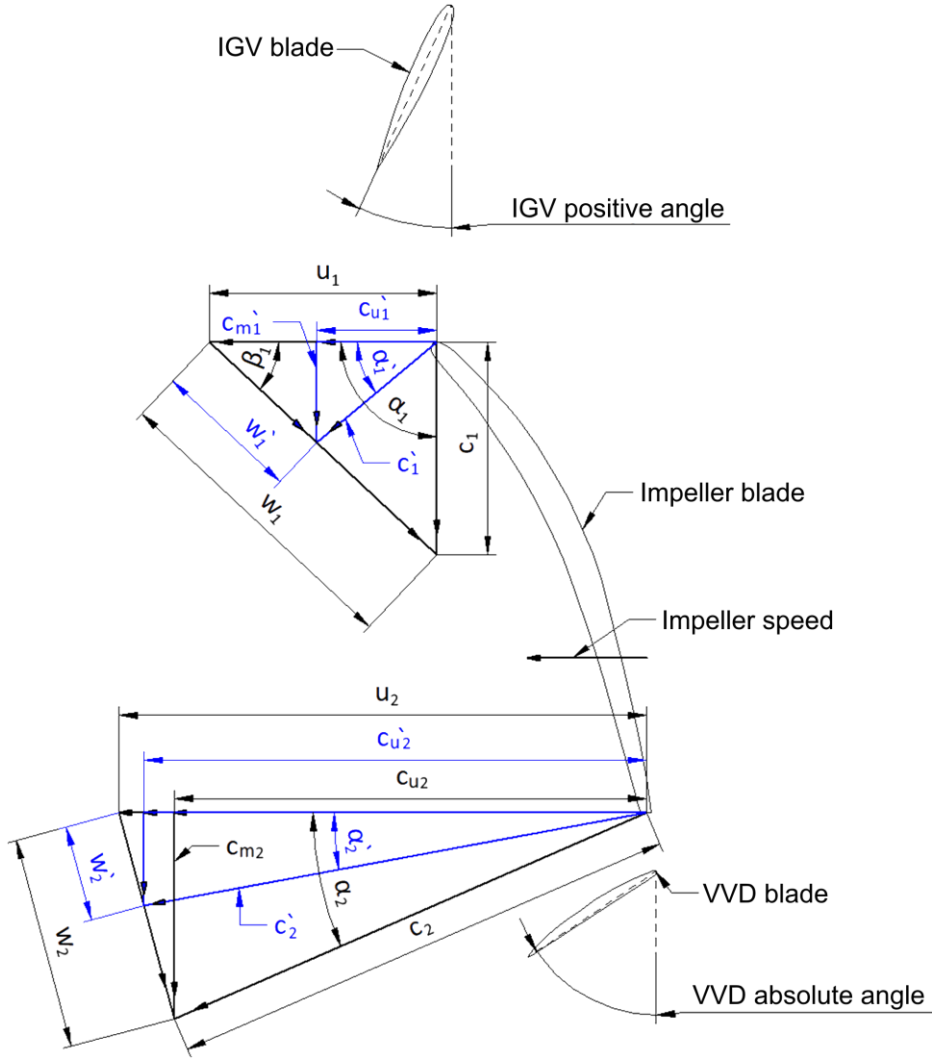

Fig. 1.2 Velocity triangles at inlet and outlet of impeller for lower flow rates than the nominal one [author's image]

In figures 1.2 and 1.3, velocity triangles at the fluid's inlet and outlet through the impeller are presented in a blade-to-blade view. The nominal operating condition is denoted by black color, while lower flow rates are depicted in blue, and higher flow rates are represented in orange.

At flow rates lower than the reference, the absolute velocity ***c*** will decrease and take the value ***c`***. In the flow, a fluid pre-rotation in the direction of the impeller's rotation given by the tangential velocity $c_u$` will occur.

Consequently, separations will appear on the pressure side of the aerodynamic profile. To eliminate the separation effect created by the difference in angle between the impeller's angle β_1 and the flow angle β_1`, the angle of the IGV blades must be modified so that those two angles β_1 regain the same value.

The absolute angle of the VVD blades refers to the positioning angle carried by the aerodynamic profile relative to the radial plane.

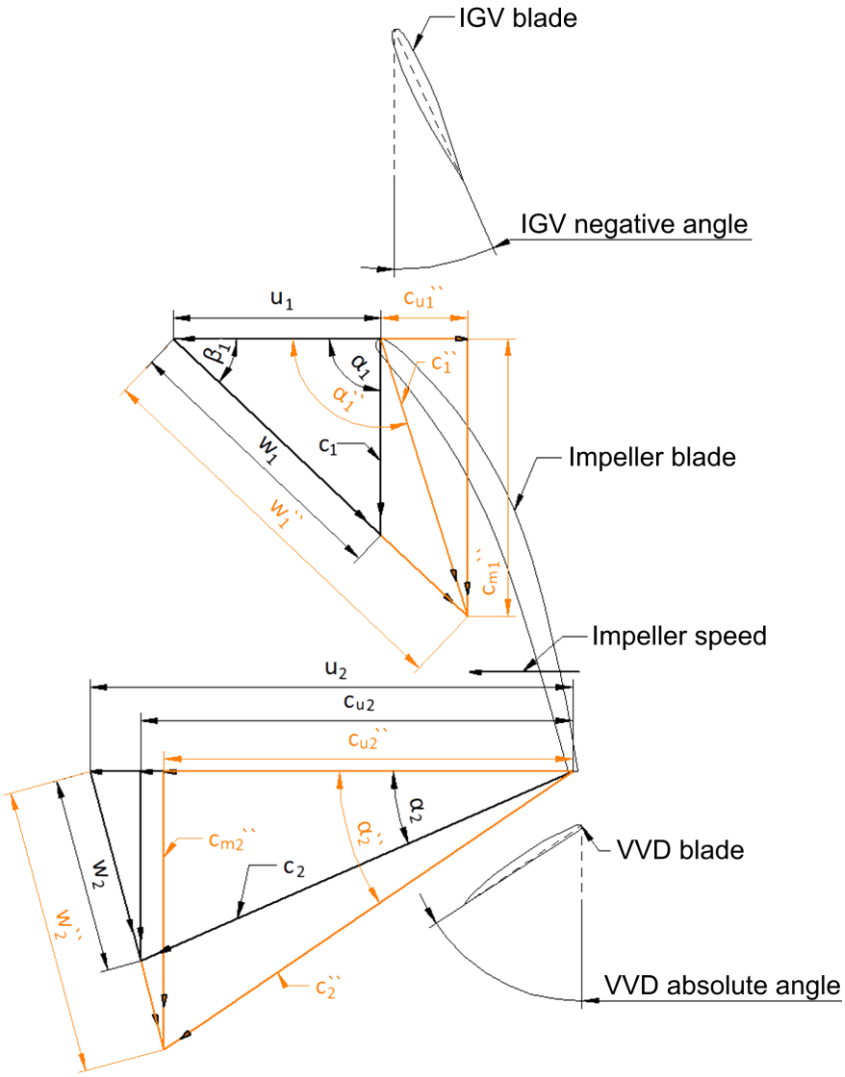

Fig. 1.3 Velocity triangles at inlet and outlet of impeller for higher flow rates than the nominal one [author's image]

At flow rates higher than the reference, the absolute velocity ***c*** will increase and take the value ***c``***. In the flow, a fluid counter-rotation opposite to the impeller's rotation direction given by the tangential component of velocity $c_u$`` will occur.

Similarly to the case presented above, to eliminate the effect caused by the appearance of this velocity component (elimination of the fluid counter-rotation effect), the angle of the IGV blades must be changed until the geometric angle β_1`` is equal to the flow angle β_1.

In summary, positive angles of the IGV are advantageous in conditions where flow rates and pressures are below nominal, while negative angles of the IGV are advantageous in conditions where flow rates and pressures exceed nominal levels.

At the exit of the impeller, at the nominal point, the inclination angle of the VVD blades will consistently align with the angle at which the fluid exits the impeller, referred to as angle α_2, provided the radial distance between the impeller and VVD blades remains small. Consequently, at higher or lower flow rates, the blades will tilt in the direction of flow (towards angle α_3 at the entry into the VVD).

1.2. Flow rate adjustment in centrifugal blowers

One of the most common applications of centrifugal blowers is to inject air into the basins of wastewater treatment plants to sustain the bacteria that perform part of the purification processes.

The machines used for these tasks are designed to maintain a constant pressure at the discharge point, considering both the pressure from the basin depth and any losses along the pipeline route.

In wastewater treatment plants, the primary factor dictating the required airflow is the concentration of oxygen in the wastewater. This is the most important parameter because air injection is conducted to sustain the existing bacteria.

If the oxygen level drops below the ideal threshold, bacteria start to die, which compromises the purification process. Conversely, if more air is pumped into the tanks, the oxygen level reaches a maximum concentration, leading to unnecessary energy consumption. Thus, the overall efficiency of the treatment plant decreases significantly.

Recognizing the importance of maintaining an optimal oxygen level in the water, G. Burger et al. [5] graphically depicted (Figure 1.4) the variation of the airflow injected into the aeration tanks of the treatment plant they analyzed over a period of about 6 months.

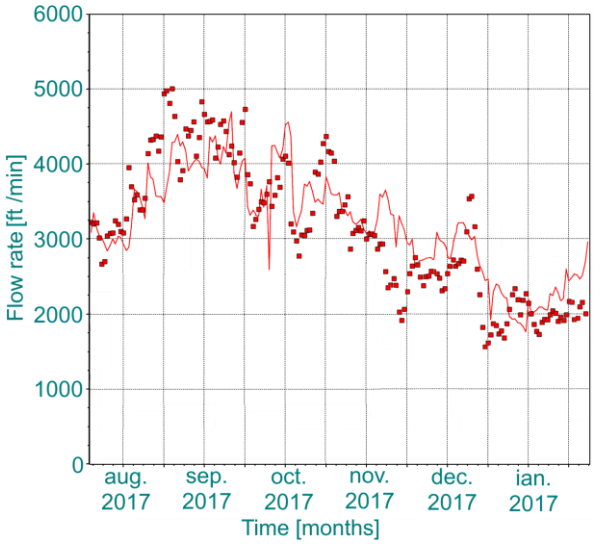

Fig. 1.4 The variation of the injected airflow into the aeration tanks over a period of six months, reproduced from [5]

A similar graph, to the one presented earlier, was created by T. Jenkins [8], but in this one, the variation of the airflow is depicted for a single aeration tank over a single day (Figure 1.5). Therefore, one can observe the airflow evolution throughout the entire day.

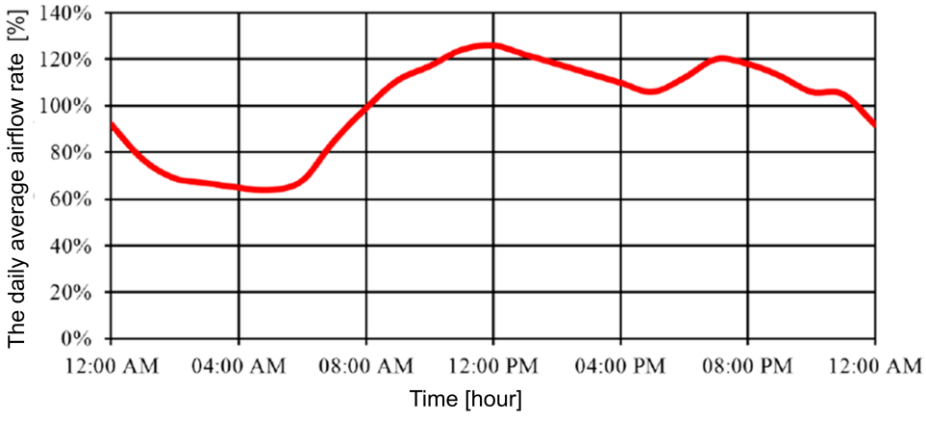

Fig. 1.5 The variation of the injected airflow into the aeration tanks in one day, reproduced from [8]

In technical applications, the most commonly used methods to adjust the airflow rate in centrifugal blowers are as follows [6], [10]:

- Reducing the flow area using a butterfly valve;
- Recirculating the airflow to decrease the air intake into the basins;
- Changing the operating speed;
- Using adjustable geometries (assisted by IGV and VVD).

CHAPTER 2 Centrifugal Blowers Design

The present chapter introduces a calculation method, developed by applying velocity triangles at the inlet and outlet of the impeller (Figure 2.1), which helps in pre-sizing or even fully sizing the main aerodynamic components of centrifugal blowers. For a much clearer understanding of the formulas used, the chapter provides a sizing example for a blower with the following operating parameters: Compression ratio: 0.6 (π_c = 1.6); Nominal flow rate: 3500 m^3/h; Working fluid: air; Suction pressure: 101 325 Pa; Suction temperature: 20 °C.

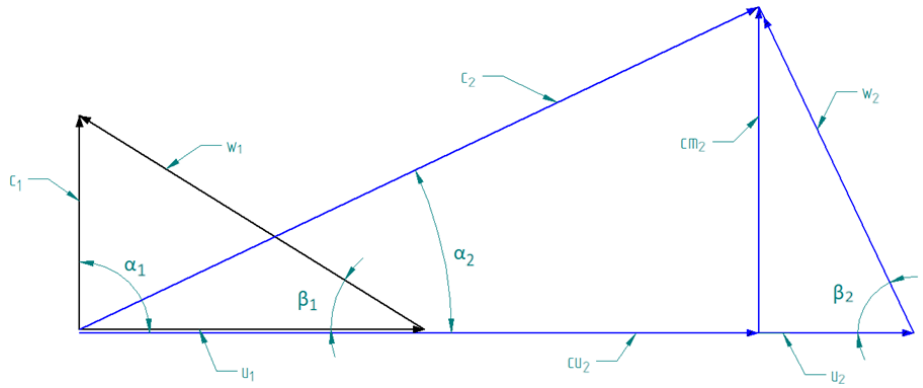

Fig. 2.1 Velocity triangles at the inlet (suffix „1") and (suffix „2") of the impeller [author's image]

The main results obtained through the application of the formulas presented in this chapter are listed in tabular form as follows (Table 2.1):

*Table 2.*1 *The data obtained for the impeller*

Notation	Value	U.M.
Q	3500	Nm^3/h
D_0	119.7	mm
c_0	90.044	m/s
c_{m0}	90.044	m/s
P_g	59.106	kW
S_1	3.5	mm
S_2	3.5	mm
z	15	$blades$
$T_{2\,s}$	319.944	K
$T_{2\,t}$	345.485	K
$p_{0\,s}$	96438	Pa
$p_{0\,d}$	4886.5	Pa
$p_{0\,t}$	101325	Pa

Notation	Value	U.M.
$\Delta p_{m\,H2O}$	6.216	m
D_1	128	mm
c_1	94.546	m/s
c_{m1}	94.546	m/s
u_1	163.587	m/s
w_1	188.943	m/s
c_{u1}	0	m/s
α_1	90	degrees
β_1	30.03	degrees
b_1	26.6	mm
$p_{1\,s}$	95938	Pa
$p_{1\,d}$	5387.4	Pa
$p_{1\,t}$	101325	Pa

Notation	Value	U.M.
$\dot{m}$	1.172	kg/s
D_2	235.5	mm
c_2	226.427	m/s
c_{m2}	103.055	m/s
u_2	300.844	m/s
w_2	143.594	m/s
c_{u2}	201.362	m/s
α_2	27.214	$deg.$
β_2	46.148	$deg.$
b_2	10.6	mm
$p_{2\,s}$	132461	Pa
$p_{2\,d}$	40854	Pa
$p_{2\,t}$	173316	Pa

CHAPTER 3 Modeling and Simulation of Centrifugal Blower Operation

According to the literature, Computer-Aided Design (CAD) systems were created to represent real technical objects in 3D, leading to detailed analysis of them.

Initiating a Computational Fluid Dynamics (CFD) simulation starts with creating a 3D model for three-dimensional flow or a 2D model for simplified flow, which requires less computing power.

The main components of the centrifugal blower, as calculated in the previous subchapter, are the impeller (Figure 3.1) and the volute. The calculations provided the construction dimensions for these two aerodynamic components.

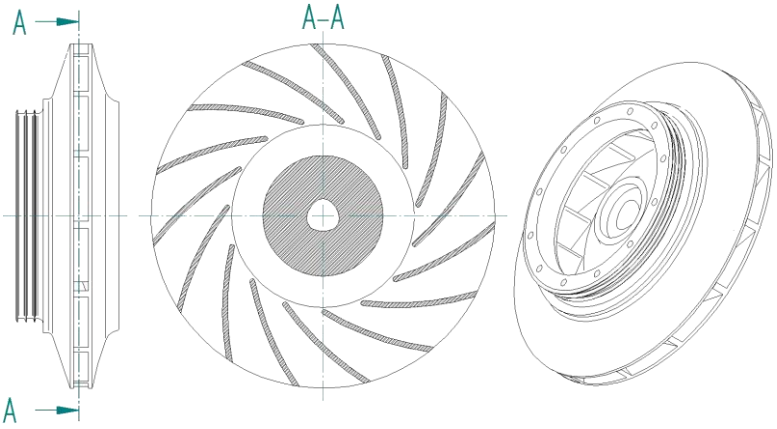

Fig. 3.1 The 2D and 3D model of the impeller [image generated by the author]

3.1. Flow simulation through the impeller

The procedure for simulating the centrifugal impeller in the ANSYS Workbench platform was executed as follows:

a) The computational domain was divided into 3 sub-domains: Geometry (where the flow channel was created), TurboGrid (where the computational grid was generated), and CFX (where boundary conditions were defined, the simulation was run and the results were verified through post-processing);

b) In order to reduce the computational power required for the CFD calculation and to minimize the run time, a single flow channel was introduced in the analysis. This resulted in a lower number of nodes and elements in the discretization;

c) In TurboGrid, the computational grid (discretization) was created and optimized. This process yielded a discretization with a total of 417 240 nodes and 394 797 elements. Moreover, to ensure high-precision results, the computational grid had a high node density in the boundary layer region.

The settings and boundary conditions used in the Ansys CFX software were as follows:

- The analysis was performed in a steady-state simulation;
- The chosen turbulence model was ***k-ω*** SST;
- The selected material was air with ideal gas properties;
- The impeller speed was set to 24 400 rpm;

- The reference pressure value was set to zero to obtain absolute pressure values in the data post-processing stage;
- For the inlet of the domain (at the entrance to the impeller), an "inlet" boundary condition was applied, with a specified absolute total pressure of p_0 = 101 325 Pa and a total temperature of t_0 = 20 degrees Celsius;
- For the outlet of the domain (at the exit from the impeller), an "outlet" boundary condition was employed, where the mass flow rate per impeller passage was used.

The convergence criteria for the residuals resulting from the iterations for the executed cases were set to a value of 1e-05. After applying all boundary conditions, the next step was to run the actual calculation of the Navier-Stokes equations. This process was stopped when a consistent pattern of certain parameters across multiple iterations was observed.

3.1.1. Results and discussions

Before analyzing the simulation results, it was essential to validate the grid refinement thoroughly. This was done through a sensitivity analysis by examining the y^+ term [4].

The optimal value of this term depends on the turbulence model used for setting up the problem. According to the data available in specialized literature, the y^+ term should be below 20 (for the SST turbulence case) to minimize the error introduced in the flow calculation near the walls (the boundary layer).

It was observed that near the blades, the y^+ value reached a maximum of 1.25, and close to the main disk, it reached a maximum of 1.47. The highest overall y^+ value was 2.24. According to the obtained and presented results, the grid refinement was validated.

The data obtained from the simulation were compiled in the table below (Table 3.1), aiming to compare the analytically obtained results with those acquired through CFD analysis.

Table 3.1. Comparison of the calculated data with the results obtained from the CFD simulation

No.	Name	Notation	Calculated value	CFD analysis value	Error [%]
1	Static pressure at the inlet of the impeller	$p_{0\,s}\,[Pa]$	96 438	95 162	1.34
2	Static pressure at the outlet of the impeller	$p_{2\,s}\,[Pa]$	132 461	130 196	1.74
3	Total pressure at the inlet of the impeller	$p_{0\,t}\,[Pa]$	101 325	101 321	0.00
4	Total pressure at the outlet of the impeller	$p_{2\,t}\,[Pa]$	173 316	175 762	1.39
5	Useful power out	$P_g\,[kW]$	59.106	60,660	2.56
6	Total temperature at the inlet of the impeller	$T_{0\,t}\,[K]$	293.15	293.152	0.00
7	Total temperature at the outlet of the impeller	$T_{2\,t}\,[K]$	345.485	340.082	1.59
8	Static temperature at the inlet of the impeller	$T_{0\,s}\,[K]$	288.697	287.935	0.26
9	Static temperature at the outlet of the impeller	$T_{2\,s}\,[K]$	319.944	320.643	0.22

The percentage error presented in Table 3.1 was calculated using the formula:

$$Error = \left| \frac{Calculated\ value \cdot 100}{CFD\ analysis\ value} - 100 \right| \quad (3.1)$$

Based on the previous analysis, it can be concluded that the calculation methodology presented in Chapter 2 is accurate (the calculated values closely match those obtained from CFD numerical simulations).

3.2. Optimizing the centrifugal impeller

After the preliminary calculations in Chapter 2, the primary dimensions and size of the centrifugal impeller were determined. Subsequently, the impeller underwent further optimization using ANSYS CCD (Centrifugal Compressor Design [1]) software to improve the overall efficiency of the centrifugal blower.

The input data for the ANSYS CCD calculation program were those presented and calculated in Chapter 2 as follows: Pressure ratio: 1.6; Mass flow rate: 1.172 kg/s; Impeller speed: it was reduced to 22 800 rpm and remained constant throughout all numerical simulations in the thesis; Inlet temperature: 293.15 K; Inlet pressure: 101 325 Pa; Hub diameter D_{1h}: 60 mm; Working fluid: air; Clearance between the impeller and the volute: 0.5 mm; Shroud diameter D_{1s}: 138 mm; Number of blades (z): 15 blades; Angle β_2 : 30 degrees.

For feasibility and durability reasons, the impeller obtained from the Vista CCD program was modified using the Ansys Bladegen software [2]. During this process, adjustments were made to the blade thickness and angles.

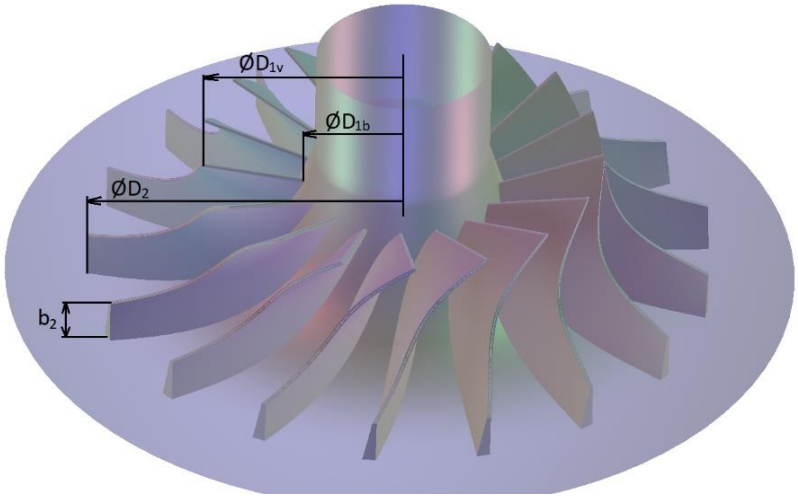

Fig. 3.2 The optimized impeller, where:
***D_{1b}** - Hub diameter at the inlet of the impeller;*
***D_{1s}** - Shroud diameter at the inlet of the impeller;*
***D_2** - Diameter at the outlet of the impeller;*
***b_2** - Blade width at the outlet of the impeller [image generated by the author]*

Thus, the preliminary results of the optimized impeller (Figure 3.2) generated by ANSYS CCD were as follows: Hub diameter D_{1h}: 60 mm; Shroud diameter D_{1s}: 138 mm; Diameter D_2 : 218 mm; Useful power out: 59.4 kW; Static pressure at the impeller outlet: 136 500 Pa; Total pressure at the impeller outlet: 168 170 Pa; Maximum Mach number: 0.711; Air temperature at the impeller outlet: 70.5 grade C.

3.2.1. Flow simulation through the optimized impeller

The current subchapter described a CFD numerical analysis of the optimized centrifugal impeller, utilizing the NUMECA Fine Turbo software [3], to validate the previously obtained data. To create the necessary computational grid for numerical simulations, the impeller geometry, generated from the ANSYS BladeGen program, was exported to the NUMECA AutoGrid program.

After inputting the following parameters into the program: selecting the curve from the impeller's hub and shroud, choosing the blade, setting the clearance between the volute and the impeller, refining the discretization etc., a fully structured computational grid was generated (composed of a single flow channel) with approximately 1.1 million nodes.

For verifying the impeller's performance and plotting characteristic curves at constant speed, CFD flow simulations were conducted with the following boundary conditions:

- The analysis was performed in a steady-state simulation;
- The mathematical model is based on the Navier-Stokes equations;
- Turbulence model used: SST;
- Reference pressure: 101 325 Pa;
- Reference temperature: 293 K;
- Working fluid: air;
- Impeller speed: 22 800 rpm;
- At the inlet of the domain, the total absolute pressure was imposed with a value of 101 325 Pa and the absolute temperature with a value of 293 K;
- At the outlet of the domain, mass flow rate was used: initially, the nominal mass flow rate of 1.172 kg/s was employed, after which, for constructing the characteristic curve, it was varied between two limits, surge and choke.

Once all boundary conditions were input, the iterative calculation process of the Navier-Stokes equations began for the given scenario. Iterations stopped when consistency was noticed in certain parameters (such as the continuity equation, efficiency, pressure increase etc.) over several iterations.

The maximum global value of the y+ term was 1.8, confirming the grid refinement.

After examining the results, noticeable enhancements in the impeller were observed. The separation that was initially present at the leading edge of the impeller (Subchapter 3.1) is no longer there, and now the fluid flows smoothly across the entire aerodynamic profile without any separation.

Using data extracted from numerical simulations, characteristic curves at constant speed were constructed (Figures 3.3 and 3.4) for the optimized centrifugal impeller, generated with the help of the new calculation programs. It was observed that at the boundaries of normal operation parameters, the two points, surge and choke, are found.

These occur at flow rates of 0.700 kg/s (where the pressure ratio is 1.690) and 1.822 kg/s (where the pressure ratio is 1.367), respectively.

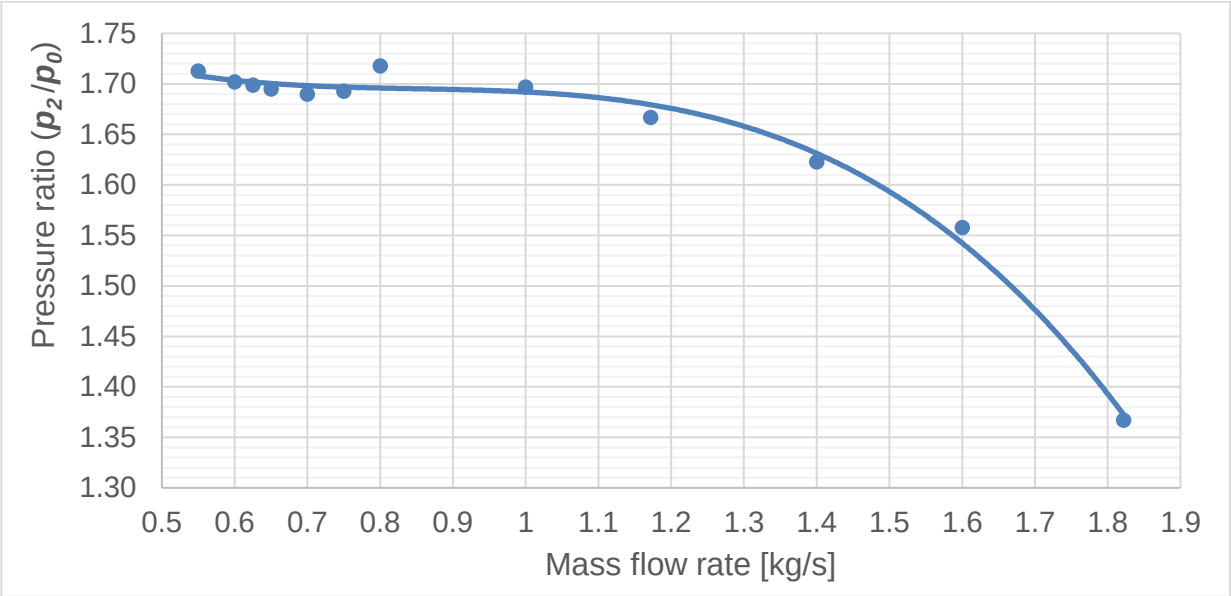

Fig. 3.3 Characteristic curve – Pressure ratio p_2 / p_0 versus mass flow rate – simulated results – [author's image]

The maximum efficiency value was 91.56%, which could decrease by up to 23% at the periphery of the stable operating range, near the choke limit.

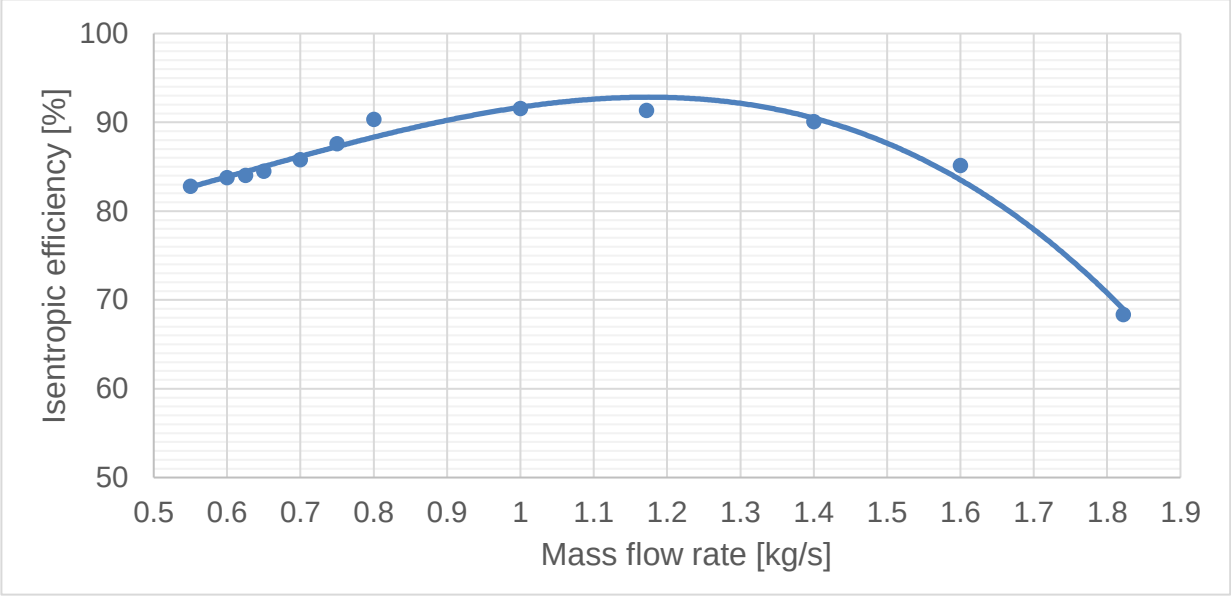

Fig. 3.4 Characteristic curve – Isentropic efficiency versus mass flow rate – simulated results – [author's image]

To create an energy-efficient centrifugal blower while adjusting the mass flow rate with consistent pressure, two distinct types of blades were installed: inlet guide vane (IGV) positioned before the impeller and variable vane diffuser (VVD) positioned after it.

3.3. Designing the Inlet Guide Vanes (IGV)

The Inlet Guide Vanes (IGV) (Figure 3.5), further abbreviated as IGV, consist of blades positioned upstream of the impeller, arranged radially. Their purpose is to direct the airflow entering the impeller.

In this subchapter, a symmetrical blade with an aerodynamic profile was constructed based on the following assumptions: feasibility, cost-effectiveness and increased precision in controlling the manufactured part. Considering all recommendations from the literature regarding the shape, position and number of blades, the geometry of the IGV blade was defined using the ANSYS BladeGen program.

3.3.1. Flow simulation through the IGV and the optimized impeller

To create the grid used in the following numerical simulations, the geometries of both the IGV blade and the impeller, obtained using the ANSYS BladeGen program, were exported to the NUMECA AutoGrid program.

For the purpose of numerically simulating the IGV + impeller assembly to analyze the influence of stator blades at different angles, several discretization were generated using the same grid generation program settings, with the only modified parameter being the IGV blade angle. Thus, 10 discretization were created, with the IGV angle varying as follows: $\sphericalangle IGV \in [-30°; -20°, \ldots, +60°]$. The computational grids obtained consisted of approximately 1.1 million nodes for the impeller domain and around 0.8 million nodes for the IGV domain.

Figure 3.5 shows the geometry of the IGV for various blade inclinations, defining both negative and positive inclinations of the IGV blades.

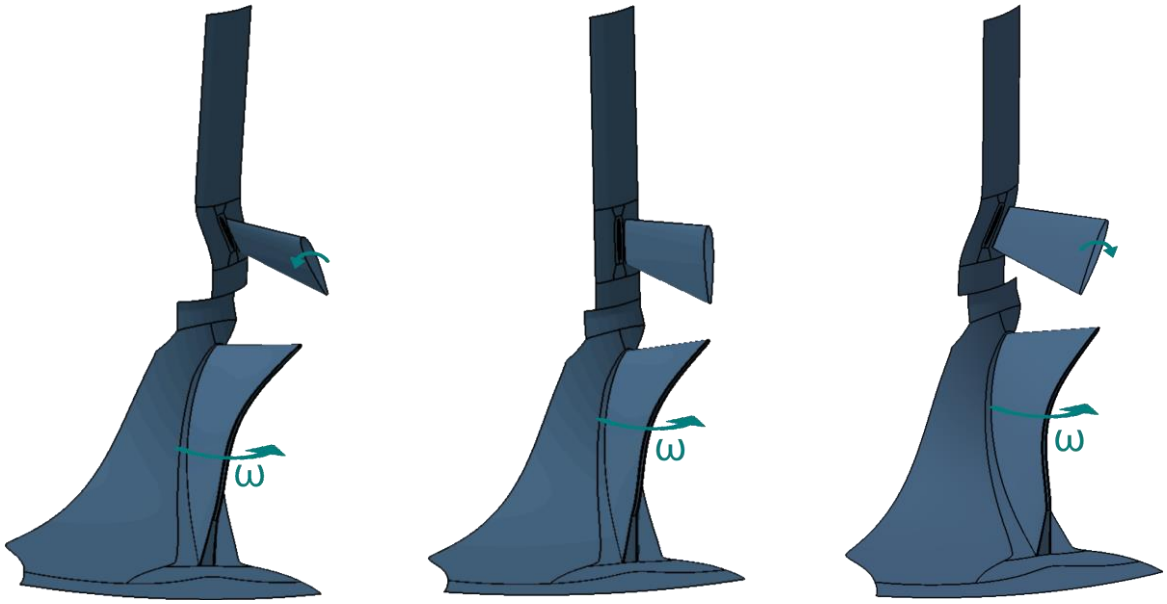

IGV angle = +30 degrees *IGV angle = 0 degrees* *IGV angle = -30 degrees*

Fig. 3.5 Rotation of the IGV blade [image generated by the author]

Positive rotations of the IGV occur when the stator blade rotates in the same direction as the centrifugal impeller during operation. Additionally, a 0-degree IGV angle is considered when the blade profile chord is positioned parallel to the suction pipe.

The boundary conditions applied in the NUMECA Fine Turbo program were the same as those used in Subsection 3.2.1. After applying all boundary conditions, iterative calculations of the Navier-Stokes equations were conducted for the specified case. Iterations were stopped upon observing repeatability of certain parameters (pressure increase, efficiency, continuity equation etc.) over several iterations. The maximum global value of the ***y+*** term was 2.25, confirming the validation of the grid refinement.

3.3.2. Results: tables and graphs

The data extracted from the numerical simulations presented above are listed in the table below (Table 3.2).

Table 3.2 Simulation Results of IGV + Impeller at Different Inclinations of the IGV Blades

No.	Mass flow rate [kg/s]	p_2/p_0 [-]	Efficiency [%]	Power [kW]	IGV angle [°]	VVD angle [°]	Relative VVD angle [°]
1	0.625	1.700	83.22	36.20	0	-68.26	-6.4
2	0.700	1.696	85.48	39.40	0	-68.64	-6.8
3	0.800	1.724	89.78	44.29	0	-69.50	-7.6
4	1.000	1.696	90.93	52.93	0	-66.07	-4.2
5	**1.172**	**1.663**	**90.70**	**59.71**	**0**	**-61.88**	**0.0**
6	1.400	1.616	89.33	68.09	0	-55.62	6.3
7	1.600	1.551	85.63	73.94	0	-48.65	13.2
8	1.817	1.368	68.01	74.95	0	-35.15	26.7
9	0.600	1.705	83.28	34.69	+10	-68.38	-6.5
10	0.650	1.697	84.72	36.82	+10	-68.62	-6.7
11	0.700	1.699	86.94	38.82	+10	-69.51	-7.6
12	0.800	1.704	90.33	43.02	+10	-69.97	-8.1
13	1.000	1.666	90.97	50.95	+10	-65.61	-3.7
14	**1.172**	**1.631**	**90.58**	**57.35**	**+10**	**-61.45**	**0.4**
15	1.400	1.574	88.58	64.73	+10	-54.72	7.2
16	1.600	1.497	83.53	69.43	+10	-47.03	14.8
17	1.762	1.340	66.87	68.74	+10	-36.37	25.5
18	0.600	1.701	84.23	34.31	+20	-69.48	-7.6
19	0.650	1.706	86.33	36.36	+20	-69.90	-8.0
20	0.725	1.698	89.46	39.04	+20	-70.88	-9.0
21	0.800	1.687	90.63	41.95	+20	-70.52	-8.6
22	1.000	1.641	90.91	49.38	+20	-65.90	-4.0
23	**1.172**	**1.602**	**90.22**	**55.30**	**+20**	**-61.17**	**0.7**
24	1.400	1.532	87.29	61.55	+20	-53.85	8.0
25	1.600	1.433	79.15	64.94	+20	-44.71	17.2
26	1.691	1.308	64.29	62.79	+20	-37.95	23.9
27	0.600	1.699	85.11	33.83	+30	-70.16	-8.3
28	0.700	1.696	89.41	38.39	+30	-71.58	-9.7
29	0.800	1.696	90.72	42.79	+30	-70.76	-8.9
30	1.000	1.568	88.73	46.37	+30	-65.71	-3.8
31	**1.172**	**1.547**	**87.52**	**56.56**	**+30**	**-60.56**	**1.3**
32	1.300	1.511	83.68	56.73	+30	-56.16	5.7

No.	Mass flow rate [kg/s]	p_2/p_0 [-]	Efficiency [%]	Power [kW]	IGV angle [°]	VVD angle [°]	Relative VVD angle [°]
33	1.400	1.461	80.45	58.02	+30	-52.49	9.4
34	1.598	1.281	59.21	57.97	+30	-41.21	20.7
35	1.600	1.259	56.67	56.83	+30	-36.91	25.0
36	0.700	1.632	87.71	38.32	+40	-71.35	-9.5
37	0.800	1.585	88.76	40.04	+40	-70.43	-8.6
38	0.900	1.633	88.81	49.11	+40	-68.73	-6.9
39	1.000	1.567	86.33	46.89	+40	-65.52	-3.6
40	**1.172**	**1.492**	**82.02**	**50.52**	**+40**	**-59.70**	**2.2**
41	1.300	1.424	76.77	53.75	+40	-54.45	7.4
42	1.472	1.252	54.59	52.07	+40	-44.55	17.3
43	0.400	1.726	80.99	24.14	+50	-74.58	-12.7
44	0.500	1.702	83.83	28.58	+50	-72.42	-10.5
45	0.600	1.676	85.65	32.83	+50	-71.37	-9.5
46	0.700	1.640	86.11	36.63	+50	-70.23	-8.4
47	0.800	1.603	86.25	39.47	+50	-70.40	-8.5
48	0.900	1.551	84.34	43.02	+50	-68.03	-6.2
49	1.000	1.495	80.37	44.08	+50	-64.58	-2.7
50	**1.172**	**1.384**	**71.80**	**46.77**	**+50**	**-57.47**	**4.4**
51	1.320	1.231	49.94	47.73	+50	-49.42	12.5
52	0.400	1.714	81.46	23.69	+60	-74.60	-12.7
53	0.500	1.681	83.23	28.01	+60	-72.18	-10.3
54	0.600	1.646	83.52	32.16	+60	-70.47	-8.6
55	0.700	1.601	83.38	35.84	+60	-70.10	-8.2
56	0.800	1.541	80.62	38.35	+60	-69.60	-7.7
57	0.900	1.471	75.70	40.33	+60	-66.68	-4.8
58	1.000	1.392	69.50	43.17	+60	-62.48	-0.6
59	1.147	1.211	44.92	41.66	+60	-53.93	7.9
60	**1.172**	**1.174**	**38.19**	**42.64**	**+60**	**-49.45**	**12.4**
61	0.700	1.695	84.23	39.90	-10	-68.02	-6.1
62	0.800	1.732	88.87	45.20	-10	-68.90	-7.0
63	1.000	1.722	90.55	54.77	-10	-65.89	-4.0
64	**1.172**	**1.696**	**90.58**	**62.29**	**-10**	**-62.22**	**-0.3**
65	1.400	1.655	89.54	71.60	-10	-56.34	5.5
66	1.600	1.603	87.03	78.58	-10	-50.19	11.7
67	1.870	1.395	68.02	82.09	-10	-34.45	27.4
68	0.700	1.692	83.10	40.42	-20	-67.40	-5.5
69	0.800	1.728	87.32	45.79	-20	-68.31	-6.4
70	1.000	1.739	89.45	56.59	-20	-65.28	-3.4
71	**1.172**	**1.722**	**89.70**	**64.85**	**-20**	**-61.84**	**0.0**
72	1.400	1.689	88.78	75.28	-20	-56.58	5.3
73	1.600	1.652	86.95	84.02	-20	-51.44	10.4
74	1.904	1.412	65.33	88.87	-20	-34.03	27.8
75	0.700	1.684	81.03	40.92	-30	-66.70	-4.8
76	0.800	1.727	84.53	45.72	-30	-67.16	-5.3
77	0.900	1.728	86.22	51.00	-30	-67.30	-5.4
78	1.000	1.729	86.67	59.21	-30	-65.25	-3.4
79	**1.172**	**1.715**	**85.91**	**67.19**	**-30**	**-60.81**	**1.1**
80	1.400	1.693	84.12	79.72	-30	-55.70	6.2
81	1.600	1.672	81.74	93.00	-30	-50.80	11.1
82	1.891	1.416	60.09	98.27	-30	-34.92	27.0

By merging all the data into a single table, including the different tilts of the IGV blades, it becomes clear how this variable influences and modifies the operating parameters of the centrifugal blowers.

The rows in bold represent the points simulated at the nominal mass flow rate of 1.172 kg/s. This aids in comparing the differences at various IGV blade tilts, specifically in terms of discharge pressure, efficiency, power consumption and the optimal angles for placing the VVD blades to minimize pressure losses.

To maximize efficiency, the VVD blade angle should align with the average α_2 angles (angles of all fluid particles at the same diameter, formed where absolute velocity intersects transport velocity) at the impeller exit.

Therefore, by analyzing this data, relationships can be established between various variables based on the tilt of the IGV blades. This detailed understanding is essential for optimizing blower efficiency according to specific operational requirements.

Presented graphically, the data shown earlier construct characteristic curves (pressure rise and efficiency versus mass flow rate) at a constant speed.

Figures 3.6 and 3.7 display the main characteristic curves, illustrating that as the IGV tilt angle increases, operational parameters decrease. Specifically, for the same discharge pressure, the flow rate decreases. Conversely, negative IGV tilts showed increases in operational parameters.

Therefore, it is observed that the change in the angle of the IGV blades directly and significantly affects both the pressure ratio (p_2/p_0) and the airflow delivered by the blower.

Lower flow rates than the nominal one (↘) are compressed more efficiently at positive stator tilts, while higher flow rates than the nominal one (↗) are achieved more effectively at negative tilts (Figures 3.8 and 3.9).

Additionally, adjusting the IGV blades noticeably expands the stable operating range of the blower. Figure 3.6 compares the operating points achieved with the IGV blades set at 0 degrees and positive stator tilts, while Figure 3.7 presents the same comparison with negative tilts used.

The surge limit is located at the start of each curve (left end, where the flow rate is minimal), while the choke limit is located at the opposite end (right end, at maximum flow rate).

An important aspect observed in the efficiency characteristic curves (Figures 3.8 and 3.9) is that the highest efficiency is located at the nominal point (mass flow rate = 1.172 kg/s), where the IGV blades are set to the "fully open" position.

Furthermore, at high angles of incidence set for the IGV blades, separation will consistently occur following fluid interaction with the aerodynamic profiles. In the simulated scenario, the minimum recorded efficiency was 38.2%.

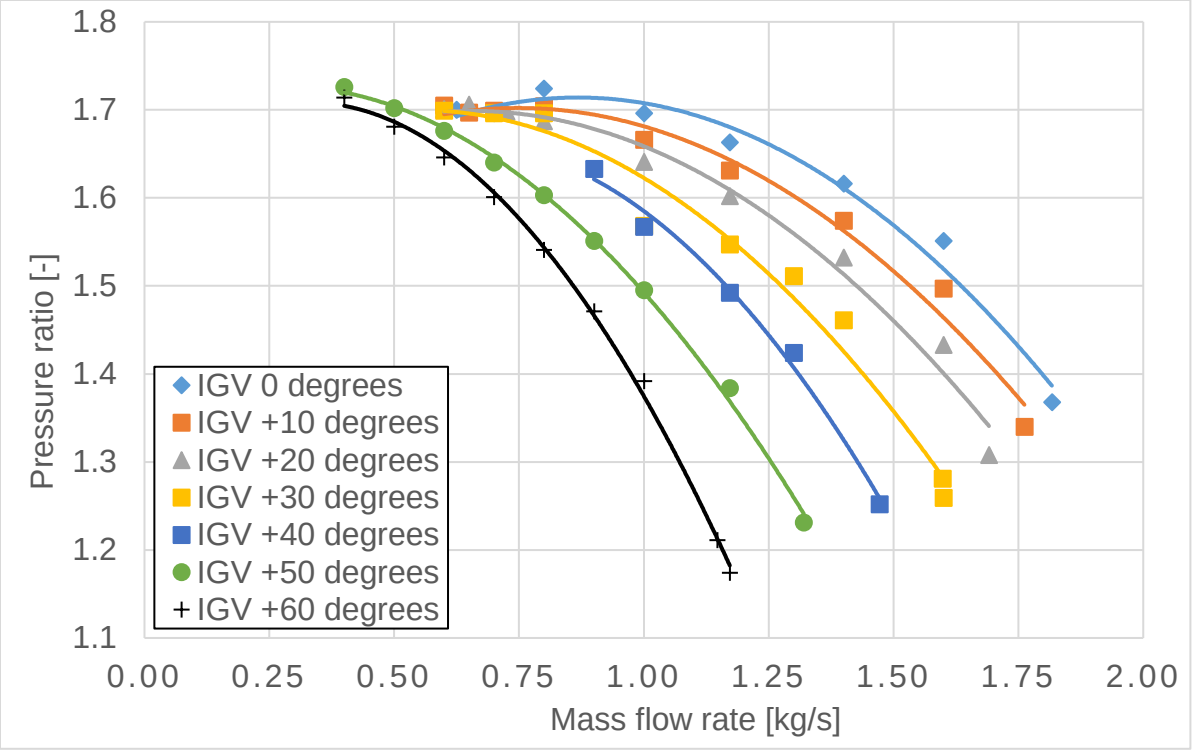

Fig. 3.6 Pressure ratio versus mass flow rate – lower flows rate than the nominal one [author's image]

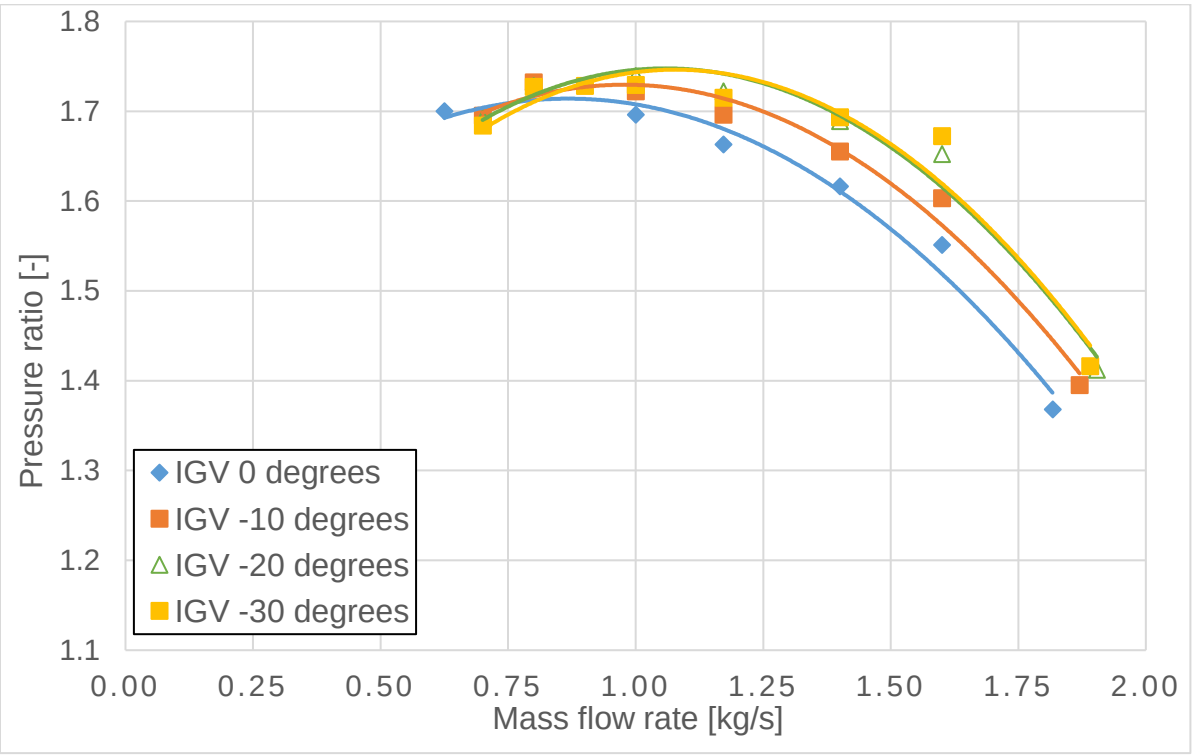

Fig. 3.7 Pressure ratio versus mass flow rate – higher flows rate than the nominal one [author's image]

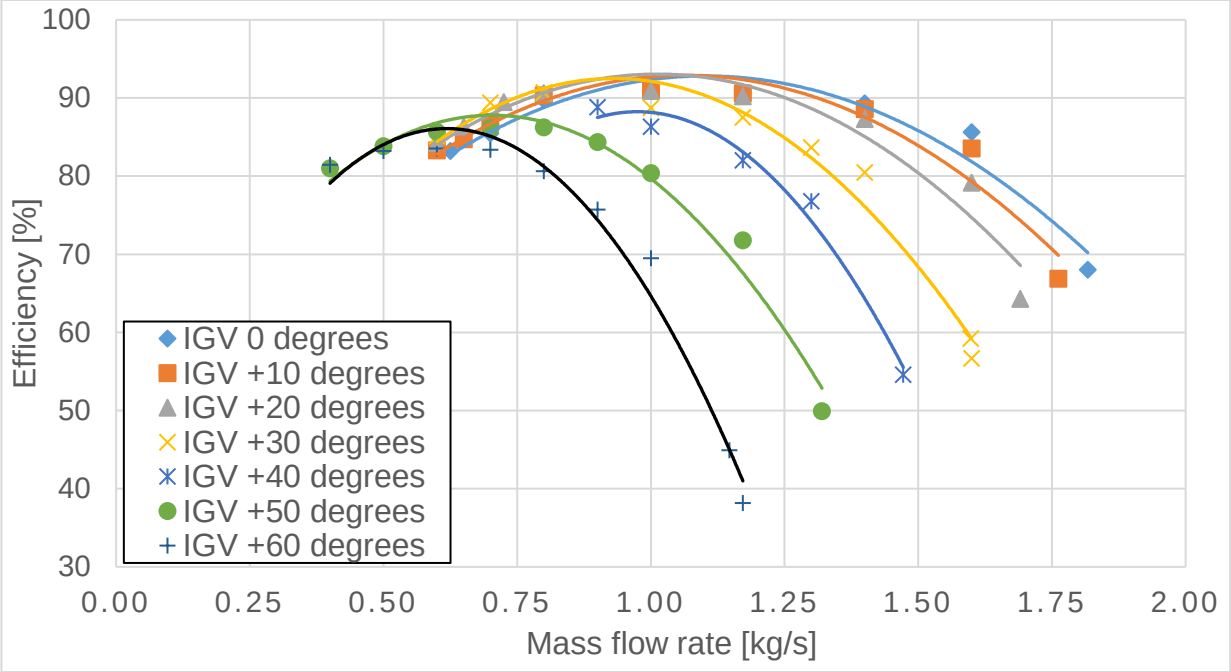

Fig. 3.8 Efficiency versus mass flow rate – lower flows rate than the nominal one [author's image]

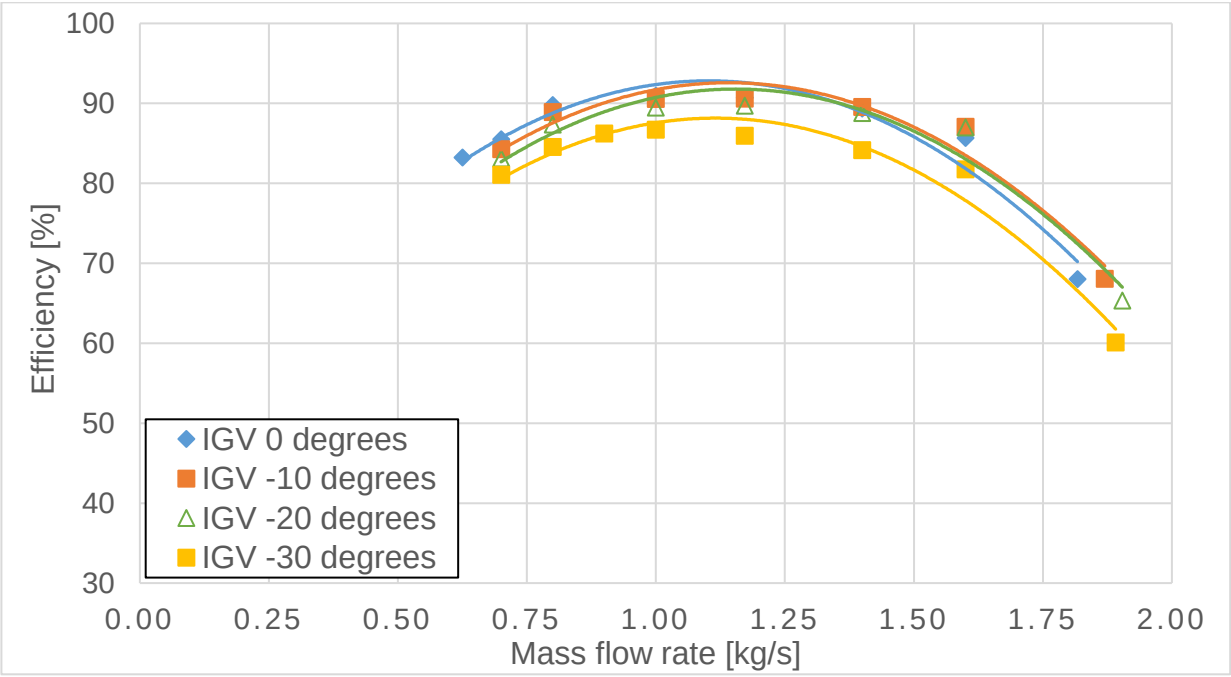

Fig. 3.9 Efficiency versus mass flow rate – higher flows rate than the nominal one [author's image]

Based on the data collected, a graph (Figure 3.10) was created to illustrate how the angle of the VVD blades depends on the angle of the IGV blades to maintain constant pressure at maximum efficiency.

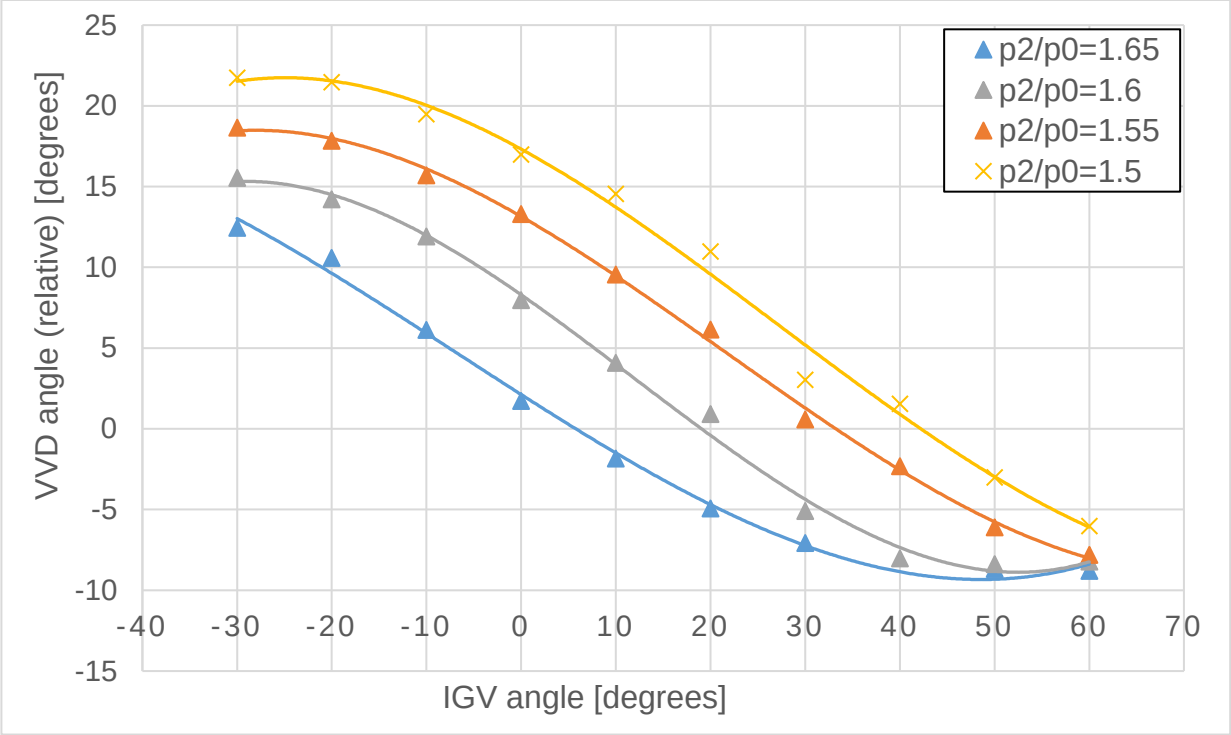

Fig. 3.10 ∢VVD = f(∢IGV) at constant pressure and maximum efficiency [author's image]

It is observed that the shape of all constant pressure curves resembles that of a third-degree polynomial function. The corresponding equations can be approximated as follows:

- For p_2/p_0 = 1.65:

$$\sphericalangle SPR = 4E-5 \cdot \sphericalangle SAR^3 + 9E-4 \cdot \sphericalangle SAR^2 - 0.3745 \cdot \sphericalangle SAR + 2.1244 \quad (3.2)$$

- For p_2/p_0 = 1.6:

$$\sphericalangle SPR = 9E-5 \cdot \sphericalangle SAR^3 - 3{,}1E-3 \cdot \sphericalangle SAR^2 - 0.4082 \cdot \sphericalangle SAR + 8.3002 \quad (3.3)$$

- For p_2/p_0 = 1.55:

$$\sphericalangle SPR = 6E-5 \cdot \sphericalangle SAR^3 - 3{,}6E-3 \cdot \sphericalangle SAR^2 - 0.3369 \cdot \sphericalangle SAR + 13.148 \quad (3.4)$$

- For p_2/p_0 = 1.5:

$$\sphericalangle SPR = 5E-5 \cdot \sphericalangle SAR^3 - 4{,}4E-3 \cdot \sphericalangle SAR^2 - 0.321 \cdot \sphericalangle SAR + 17.321 \quad (3.5)$$

If the calculated blower is used in wastewater treatment plants, specifically for transferring oxygen from air into water, the minimum discharge pressure (load) it must provide will be dictated by the constant basin depth. Therefore, the blower needs to allow adjusting the flow to maintain a consistent pressure ratio.

An example of interpreting Figure 3.10 (based on Table 3.2) can be explained as follows: If the current operating point of the blower is at a pressure ratio of p_2/p_0 = 1.6 and a mass flow rate $\dot{m}$ = 1.179 kg/s and there's a need to increase the flow rate to 1.604

kg/s (a 36% increase), the angle of the IGV blades should change from +20 degrees to -10 degrees. At the same time, the angle of the VVD blades must adjust from +0.92 degrees (relative) to +11.91 degrees (relative). These adjustments to both stator angles ensure that maximum efficiency is maintained.

In summary, for optimal efficiency, the angle of the VVD blades should align with the angle generated by a fluid particle at their seating diameter. This ensures that the fluid particle trajectory at the impeller exit matches the VVD blade angle, preventing separation after the VVD blades' leading edge.

The simulations showed that at IGV blade angles greater than ±20 degrees, separations start to occur on the pressure or suction side of the stator blades, resulting in decreased efficiency.

3.4. Designing the Variable Vane Diffuser (VVD)

The Variable Vane Diffuser (VVD) is a device consisting of radially arranged blades located downstream of the impeller. Its purpose is to slow down the fluid so that part of the kinetic energy available at the impeller exit is converted into pressure energy.

3.4.1. Flow simulation through the IGV, optimized impeller and VVD

To obtain the calculation grid necessary for the following numerical simulations, the geometries of the IGV blade, impeller and VVD blade, created using ANSYS BladeGen, were exported to NUMECA AutoGrid. After setting the requirements in the program, computational grids (each consisting of a single flow channel between two blades) for these three aerodynamic components were generated (Figure 3.11). In total, three calculation grids were created as follows:

- A grid where the VVD blade was set at the approximate angle found and listed in Table 3.2 (point 5), which is -62 degrees;
- Two other grids where the VVD blade position was adjusted from the identified position to values plus and minus two degrees, namely -60 and -64 degrees.

The grid structure was set up as follows: the discretization of the impeller channel included approximately 1.1 million nodes, the discretization of the IGV channel included approximately 1 million nodes and the discretization of the VVD channel included approximately 0.6 million nodes.

The boundary conditions set in NUMECA Fine Turbo were the same as those used in Subsection 3.2.1, with the only difference being the mass flow rate set at the outlet, specifically fixed at 1.172 kg/s. After all boundary conditions were applied, the iterative solving of the Navier-Stokes equations for the current case was carried out. Iterations were stopped when consistent parameters were observed over several iterations.

According to the theory presented in the thesis regarding the term y^+ and analyzing the data, it is noted that its value falls within normal parameters, indicating that the

calculation grid introduces no errors in the results. The maximum global value of the y+ term is 2 (Fig. 3.11).

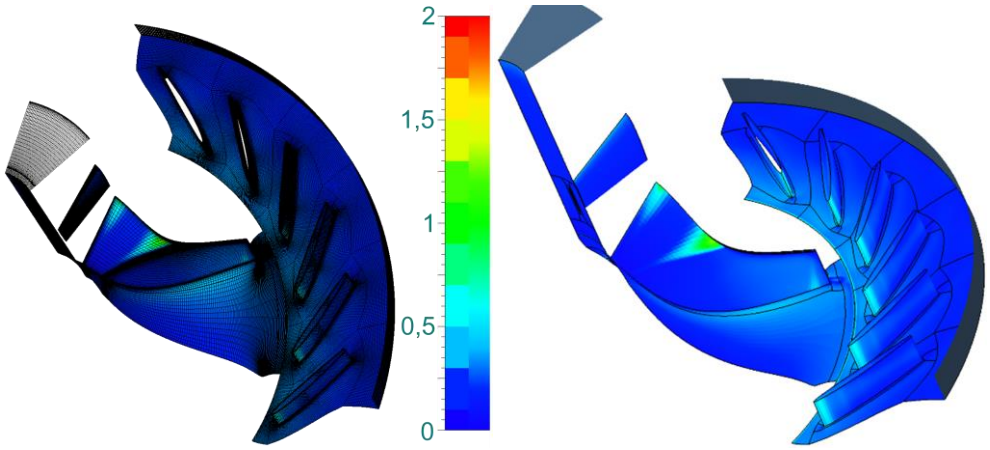

Fig. 3.11 Values of the y^+ term [image generated by the author]

Following this validation, various distributions such as total pressure, static pressure, velocity and velocity vectors were extracted using the CFView program. Analysis of the relative velocity vectors revealed no separations in the streamlines at the simulated nominal operating point.

After the simulation, it was found that at the nominal flow rate of 1.172 kg/s, the centrifugal blower can achieve an absolute pressure ratio of 1.643 with an efficiency of 88.89%. The power required in this case was 60 kW.

Using the same simulation setup (applying identical boundary conditions) for the other two grids created earlier (with VVD blade angles set at -60 and -64 degrees), the comparison was made regarding their efficiency in compressing the same airflow rate. This comparison provided insights into the impact of angular deviations in VVD blade positioning on performance.

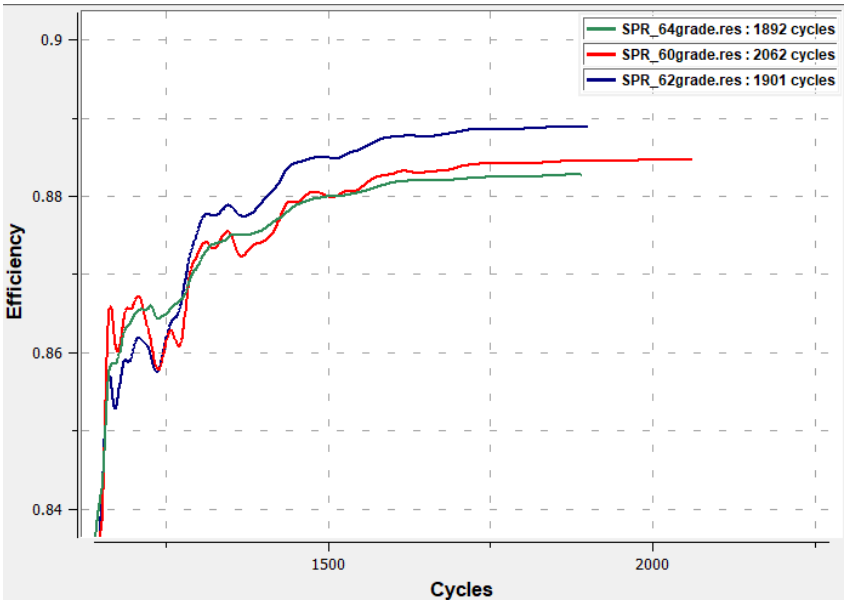

Fig. 3.12 The variation in efficiency when changing the angle of the VVD blades to one different from that presented in Table 3.2 [image generated by the author]

Figure 3.12 illustrates the efficiency evolution for each geometry based on the iteration reached in the calculation following the application of the Navier-Stokes flow equations. It was observed that the highest efficiency is achieved only when the VVD blades are aligned along the direction given by the streamlines exiting the impeller, that is, along the average angles α_2 at the impeller exit. The efficiency values for these three simulated cases are presented in the following table (Table 3.3).

Table 3.3 The efficiency values for various tilt angles of the VVD (at a flow rate of 1.172 kg/s)

The angle of the VVD blades	-60	**-62**	-64
The efficiency value	88.47%	**88.89%**	88.27%

This highlights that the maximum operating efficiency is achieved only when the VVD blades are tilted at -62 degrees and by changing this angle by two degrees, efficiency can decrease by up to 0.62%.

Therefore, the position of the blades at the nominal point will be as follows:

- The IGV blades will be positioned at zero degrees (parallel to the suction pipe);
- The VVD blades will be positioned at -62 degrees (relative to a perpendicular drawn on the outer diameter of impeller D2).

CHAPTER 4. Experimental Investigations of Centrifugal Blowers

A highly important chapter in the operation of turbomachinery is represented by the experimental measurement of parameters (mass flow rate, pressure rise, power consumption, temperature etc.) and the performance achieved by the compression unit.

Through experimental investigations, the methodology for blower sizing can be validated by comparing actual blower parameters with theoretical calculations.

On one hand, by recording the flow rate and pressure at various operating points while keeping the speed constant, the pressure ratio’s characteristic curve of the analyzed blower can be constructed. On the other hand, the main disadvantage of physical testing is that the recording instruments must be very well calibrated; otherwise, they can introduce errors. Cumulatively, these errors can reach significant values (for instance, a high error of 15 degrees in temperature probe at the inlet of a centrifugal blower can lead to an error in determining the actual head of up to 4% [12]).

Adjusting the flow rate in centrifugal blowers is a topic of great importance for maintaining high efficiency. The attention given to this aspect is driven by the influence that flow rate variation has on the total power consumption. Specifically, total efficiency is directly proportional to the total power consumed by the blower to accomplish the compression process and meet its objectives successfully. Therefore, precise adjustment of the flow rate becomes essential for optimizing the performance and efficiency of centrifugal blowers.

This chapter introduces a test rig designed to measure and analyze the aerodynamic parameters generated by the centrifugal blower. It covers the rig's

construction details, dimensional characteristics and the instrumentation used for data acquisition. Central to the setup is the centrifugal blower, with its key aerodynamic components including the impeller, the blades of both stator (IGV and VVD) and the volute.

Additionally, the blower was investigated using Computational Fluid Dynamics (CFD) analyses, where flow channels were modeled based on boundary conditions obtained from experimental investigation. Comparisons between the results validated the accuracy of the CFD simulations, facilitating extraction of the fluid behavior within the turbomachinery.

4.1. The ESC10 blower test rig

The experimental setup used in this chapter was based on the four aerodynamic components of a high-flow control turbomachine: the IGV, centrifugal impeller, VVD and volute. To validate the Computational Fluid Dynamics (CFD) simulations conducted in Chapter 3, data extracted from the experimental setup of the ESC10 blower (centrifugal blower with a capacity of 10,000 Nm^3/h), depicted in Figure 4.1, were used. These data were obtained from the INCDT Comoti archive and employed in CFD flow simulations using the same computational program (Numeca), with identical boundary conditions as those applied in Chapter 3.

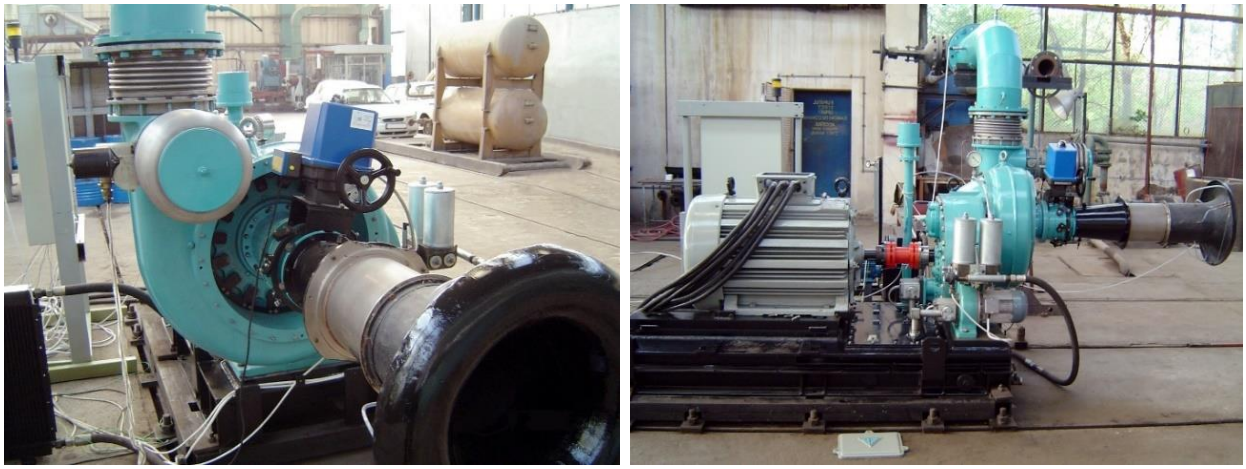

Fig. 4.1 The ESC10 blower test rig

The experimental setup diagram is shown in Figure 4.2. In this configuration, the blower draws air freely from the ambient environment through the intake duct. The angle of the inlet guide vanes (IGV) is adjusted using an electromechanical actuator, while the centrifugal impeller is driven by an electric motor via a speed multiplier. The variable vane diffuser (VVD) blades are designed to be manually rotated to the required angle for the specific flow regime. During the experimental investigation, the following parameters were recorded:

- Static pressures at the inlet (p_1) and discharge (p_5) measured via the manometers;

- The flow rate delivered by the centrifugal blower (***Q***) measured using the differential manometer connected to the Pitot tube;
- Ambient air temperature (t_0) measured using an alcohol thermometer;
- Air temperature at the inlet (t_1) and discharge (t_5) measured via thermoresistors;
- Electric current intensity absorbed by the motor (***I***) measured using an ammeter.

For additional load regulation, a manual butterfly valve is positioned on the blower's discharge pipe.

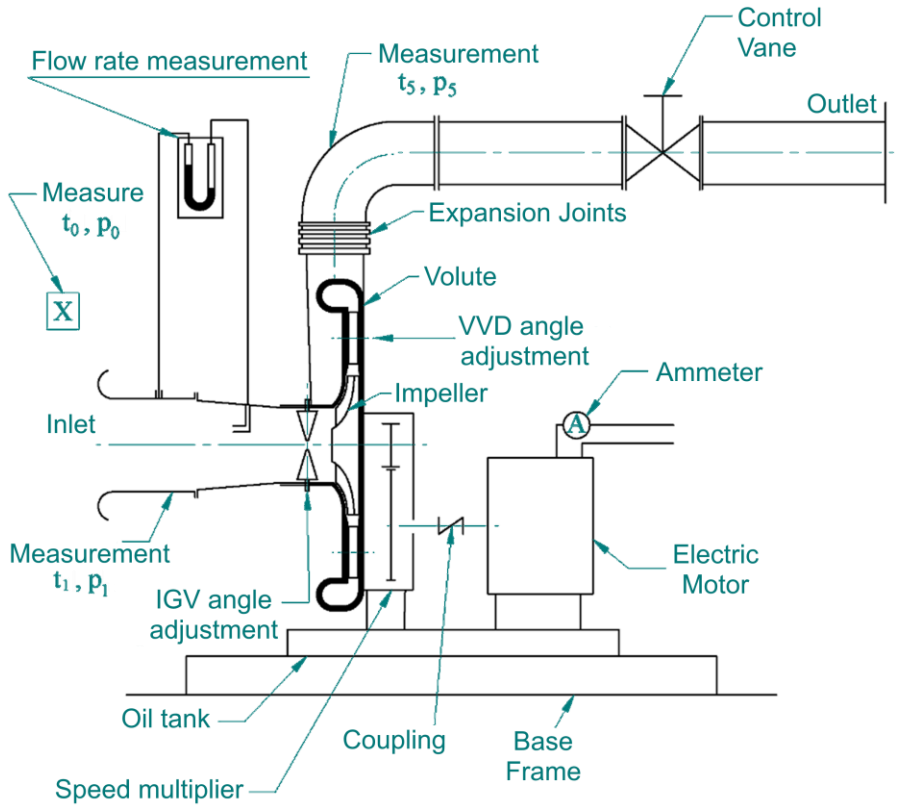

Fig. 4.2 The diagram of the ESC10 blower test rig [author's image]

4.2. Results of the experimental measurements

Figure 4.3 illustrates the direction of rotation of the SAR blades. By closing the control vane located downstream of the volute and maintaining the same angle of tilt for the IGV blades, the operating point shifts along the characteristic curve towards the surge point, resulting in a lower flow rate and higher pressure. Conversely, opening the control vane decreases the resulting head and increases the flow rate.

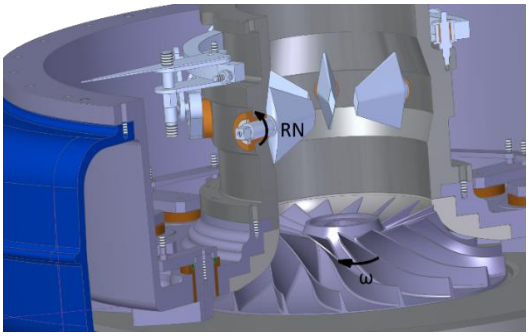

*Fig. 4.3 The inclination of IGV blades, where **RN** represents negative rotation and **ω** denotes the direction of impeller rotation [image generated by the author]*

In order to validate the numerical simulations, operating points at two different pressures were presented (Table 4.1). This approach ensures that the numerical simulations are consistent with experimental data, thereby confirming that the results obtained through numerical simulations are accurate and accurately predict the fluid behavior within the machine.

Table 4.1: Experimental measurements of ESC10.

Nr.	IGV angle [°]	VVD angle [°]	t_0 [°C]	p_5 static [bara]	t_5 [°C]	Q [Nm^3/h]	$\dot{m}$ [kg/s]	P [kW]	η [%]
1	90	0	7.5	1.7	67	10586	3.555	260	81
2	68.3	4.5	7.5	1.7	69	9764	3.279	242	83
3	54.3	8	7.5	1.7	70.5	8293	2.785	219	80
4	43	11.5	7.5	1.7	71.5	7334	2.463	201	78
5	30	16.9	7.5	1.7	73.5	6158	2.068	183	75
6	17	22	7.8	1.7	76.5	4896	1.644	160	70
7	17	22	7.8	1.6	71	5343	1.794	164	70
8	90	0	7.8	1.6	65	11995	4.028	269	80

Where the 90° angle of the IGV blades indicates a fully open position, while the 0° angle of the VVD blades represents a relative setting position compared to their position during nominal operation (the nominal point position is 50° relative to the radial direction).

4.3. Flow simulation through the ESC10 blower

The current subchapter presents a numerical CFD study on the three aerodynamic components of the ESC 10 blower: the IGV, impeller and VVD, using NUMECA Fine Turbo software [3].

To analyze the compression phenomenon and validate the performance of these three aerodynamic components, CFD simulations were conducted using identical settings to those presented in earlier chapters, with the only changes being:

- Impeller speed: 17.250 rpm;
- At the inlet: total absolute pressure: 101.325 Pa and total absolute temperature as shown in Table 4.1 (7.5°C / 7.8°C);
- At the outlet: Mass flow rate as shown in Table 4.1 (e.g. for IGV blades positioned to 90° and VVD blade positioned to 0° relative, two simulations were conducted with mass flow rates set at 3.555 and 4.028 kg/s).

To generate the calculation grids required for numerical simulations, the geometries of the IGV and VVD blades, as well as the centrifugal impeller (Figure 4.4), were reconstructed based on the manufacturing drawings used in the production process.

The 3D models were then uploaded into the mesh generation program NUMECA AutoGrid.

Fig. 4.4 The 3D geometries of these three aerodynamic components of the ESC10 blower (IGV, impeller, VVD) [image generated by the author]

After setting the program requirements (selecting the blades, selecting the blade profile at the hub and shroud of the impeller, adjusting the clearance between the impeller and the volute, refining the discretization etc.), the computational mesh was generated. It consists of a single flow channel with three subdomains: Subdomain 1 represents the flow channel between two IGV blades, Subdomain 2 represents the flow channel between two impeller blades and Subdomain 3 represents the flow channel between two VVD blades.

For the nominal case, where the IGV blade angle is 90° and the VVD blade angle is 0° relative (50° absolute), a computational mesh was generated with approximately 2.9 million nodes and 0 negative elements (the mesh was fully structured). In order to simulate all the points listed in Table 4.1, six computational grids were generated, adjusting the angles of the IGV and VVD blades based on experimental data obtained from tests conducted on the ESC10 test rig.

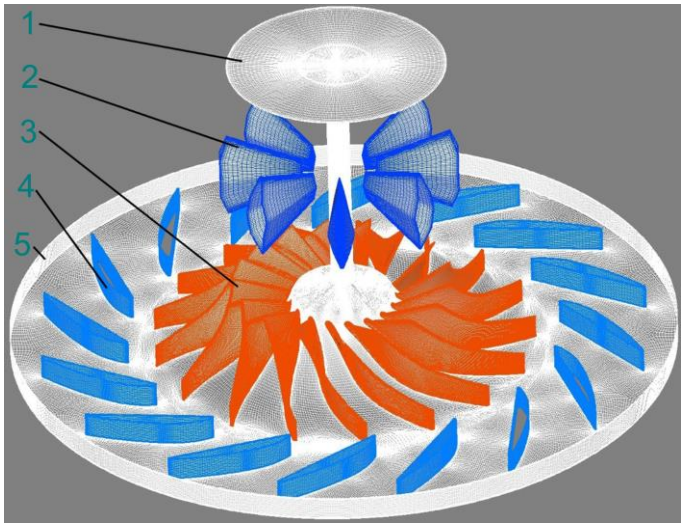

Fig. 4.5 Computational grid, where:
1 – fluid inlet; 2 – IGV blade;
3 – impeller blade; 4 – VVD blade;
5 – fluid outlet
[*image generated by the author*]

After applying the boundary conditions, the iterative solution of the Navier-Stokes equations was performed for the present case. Iterations were stopped upon observing repeatability of certain parameters across multiple iterations.

The maximum global value of the ***y+*** term was 3.5, confirming the validation of the computational grid refinement.

4.4. ESC10 blower numerical simulation results

The data extracted from the numerical simulations are presented in Table 4.2.

Table 4.2 Computational results

IGV angle [°]	VVD angle [°]	t_0 [°C]	p_4 total [Pa]	t_4 [°C]	Q [Nm³/h]	$\dot{m}$ [kg/s]	P [kW]	η [%]	p_5 static CFD [Pa]	ε_{p5s} [%]
90	0	7.5	186,235	67.2	10,586	3.555	234.5	82.02	174,254	2.50
68.3	4.5	7.5	185,019	68.9	9,764	3.279	211.4	83.31	172,366	1.39
54.3	8	7.5	181,979	69.9	8,293	2.785	182.5	79.64	170,825	0.49
43	11.5	7.5	179,548	70.7	7,334	2.463	161.6	76.96	169,359	-0.38
30	16.9	7.5	178,940	73.7	6,128	2.058	137.7	75.03	173,458	2.03
17	22	7.8	169,517	75.2	4,955	1.664	111.8	67.11	165,775	-2.49
17	22	7.8	161,411	70.9	5,342	1.794	114.6	66.71	156,676	-2.08
90	0	7.8	177,825	64.6	11,994	4.028	243.3	79.84	156,984	-1.89

In Chapter 3, several Computational Fluid Dynamics (CFD) simulations were conducted for a centrifugal blower designed to compress the flow rate to the nominal point of 1.172 kg/s. To reduce computation time, operating parameters were studied only through the three aerodynamic components (IGV, impeller, VVD), excluding the volute from the calculations.

For the purpose of validating the obtained results, this chapter presents numerical simulations conducted using an experimentally tested blower (ESC10). These simulations include identical boundary conditions and replicate the simulation approach used in the previous chapter, with the only modifications being the 3D geometry and the imposed outlet flow rate value in the computational domain.

Therefore, to compare the results obtained from numerical simulations of the ESC10 blower with those obtained experimentally, it is necessary to calculate the static pressure at the exit of the volute casing. To achieve this, using formulas published in references [7], [9] the pressure losses along the volute were computed. This enabled the comparison of the two static pressure at the blower exit: the value obtained experimentally and that derived from the CFD flow simulations.

The calculation error regarding the static pressure at the exit of the volute was determined using the formula:

$$\varepsilon_{p5s} = \frac{p_5 s\ (CFD) \cdot 100}{p_5 s\ (Measured)} - 100 \qquad (4.1)$$

where ***p_5s (Measured)*** represents the static pressure measured during the experimental testing of the ESC10 blower, the value of which is presented in Table 4.1.

The static pressure values calculated through CFD simulations closely match those obtained experimentally (with errors in terms of pressure at the blower exit under 2.5%, deemed acceptable in engineering). This similarity underscores the validity of the results. Moreover, the theoretical RANS equations accurately predict the flow phenomena within the tested turbomachinery.

In other words, the simulations in the current chapter were conducted without significant errors and were validated with experimental measurements, using the same simulation approach as in the previous chapter. In that chapter (Chapter 3):

- the same solver program for solving the flow equations;
- identical boundary conditions;
- the same type of interface between computational domains;
- the same turbulence model;
- similar computational grids.

All these indicate that the simulations carried out in Chapter 3 are reliable and provide a highly accurate prediction of the performance of the studied centrifugal blower.

CHAPTER 5. IGV and VVD angle adjustment mechanisms

The working point of centrifugal blowers in the biological stage of wastewater treatment plants is constantly adjusted based on the required amount of oxygen for the process. Therefore, changing the airflow rate injected into the basins must be done quickly, with the essential condition of managing energy efficiently to maintain maximum efficiency levels.

The mechanisms for adjusting the angles of IGV and VVD blades are essential for precisely controlling and maintaining the blade positions. This ensures the efficient operation of the compression unit overall.

5.1. IGV angle adjustment mechanism

The IGV blades are moved using a system of levers and rings, enabling them to rotate around their axis. By adjusting these blades, their position relative to the airflow can be controlled, thereby adjusting the amount of air entering the machine.

Figures 5.1 – 5.3 illustrate a control mechanism for ensuring the stable rotational movement of IGV blades.

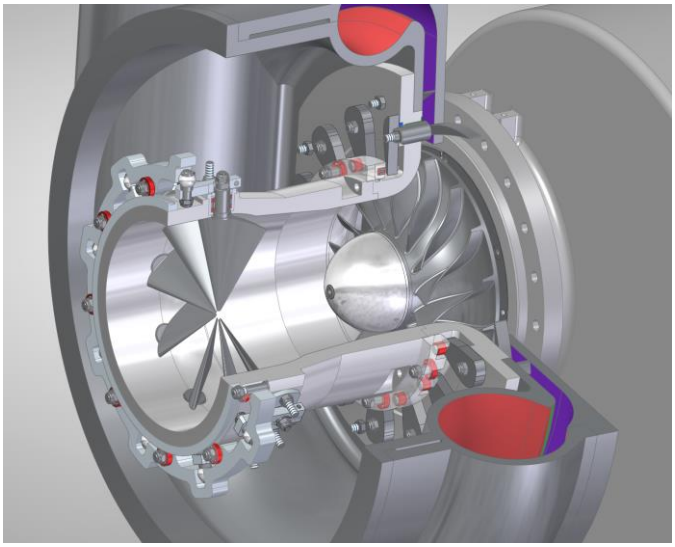

Fig. 5.1 IGV blade angle adjustment mechanism [image generated by the author]

The IGV blades ***(1)*** in Figure 5.2 are held by ball bearings ***(2)*** and feature two parallel faces (the blades' alignment mark). These ensure correct positioning during assembly and maintain a certain orientation of the blades relative to the entire mechanical adjustment system.

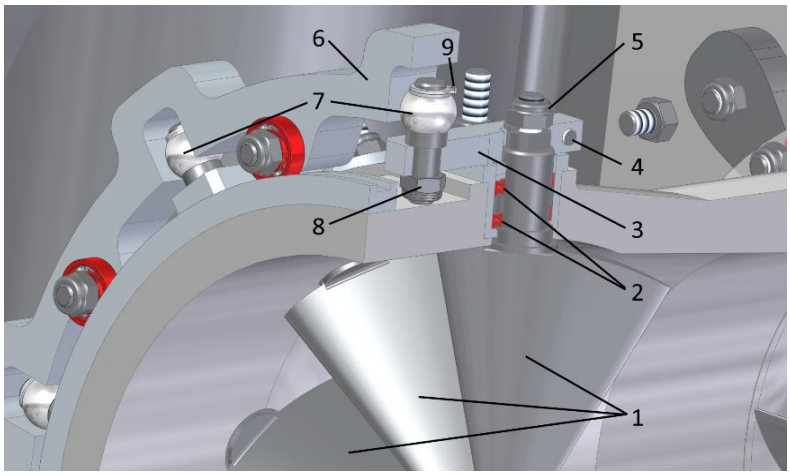

Fig. 5.2 Section through the IGV adjustment mechanism, where: 1 – IGV blade; 2 – ball bearing; 3 – lever; 4 – screw; 5 – nut; 6 – adjusting ring; 7 – spherical ball; 8 – bolt; 9 – retaining rings [image generated by the author]

The lever ***(3)*** is fixed to the blade's positioning mark by tightening the screw ***(4)*** and the axial movement of the blade is stopped by the nut ***(5)***. By rotating the adjustment ring ***(6)***, the spherical ball ***(7)***, which is attached to the lever ***(3)*** via the bolt ***(8)*** and the retaining ring ***(9)***, achieves a rotational movement centered around the IGV blade's axis

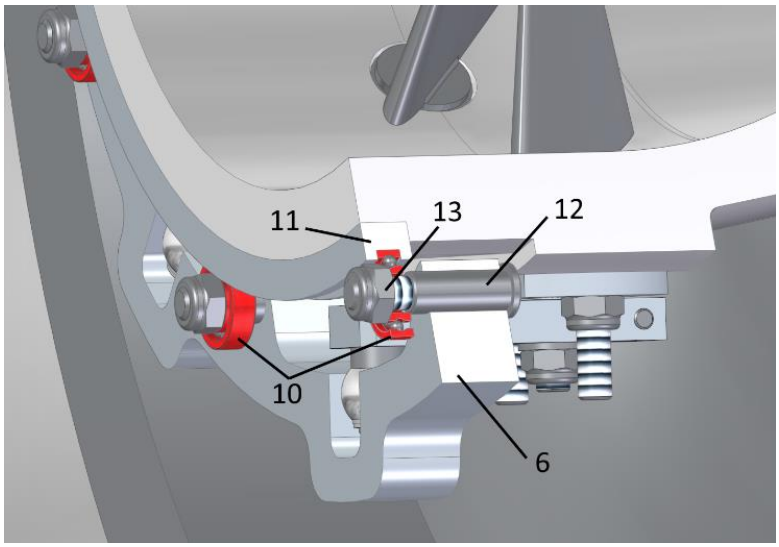

Fig. 5.3 Section through the IGV adjustment mechanism, where: 6 – adjusting ring; 10 – bearings; 11 – locking ring; 12 – bolt; 13 – nut [image generated by the author]

The adjustment ring ***(6)*** in Figure 5.3 has a rotational movement around the blower axis, being movable on the rotation axis via ball bearings ***(10)***, which rotate in the channel present in the locking ring ***(11)***. The connecting elements between components ***(6)*** and ***(11)*** are the bearings ***(10)***, bolts ***(12)*** and nuts ***(13)***. Thus, by rotating the adjustment ring ***(6)*** the tilt angle of the IGV blades can be changed, ensuring the same tilt angle for all the blades, with the only angular deviations being those resulting from the tolerances of mechanical processing.

5.2. VVD angle adjustment mechanism

The VVD blade movement mechanism operates similarly to the previously described system, employing a configuration of levers and rings that enable the blades to rotate around their axis. By controlling this rotation, the blades can be positioned within the airflow generated by the centrifugal impeller, thereby adjusting the discharge pressure exiting the machine. Figures 5.4 – 5.6 show a stable mechanism for controlling the rotational movement of the VVD blades.

The VVD blades ***(1)*** in Figure 5.5 are supported by a PTFE bushing ***(2)*** and have two parallel faces (the blade positioning mark).

These ensure correct positioning during assembly and maintain a specific orientation of the blades relative to the entire mechanical adjustment system.

The lever ***(3)*** is aligned using the blade positioning mark and the axial movement of the blade is stopped by the nut ***(4)***.

The sealing around the blade shroud passage is achieved using the sealing gasket ***(5)***.

By rotating the adjustment ring ***(6)***, the needle roller bearing ***(7)***, which is secured to the lever ***(3)*** via the bolt ***(8)***, rotates around the axis of the VVD blade.

The adjustment ring ***(6)*** in Figure 5.6 rotates around the blower axis, being movable on the rotation axis via ball bearings ***(9)***, which rotate in the channel on the impeller front cover ***(10)***.

The connecting elements between components ***(6)*** and ***(10)*** are the ball bearings ***(9)***, bolts ***(11)*** and nuts ***(12)***. Thus, by rotating the adjustment ring ***(6)*** the tilt angle of the VVD blades can be changed, ensuring the same tilt angle for all blades, with the only angular deviations resulting from tolerances in mechanical processing.

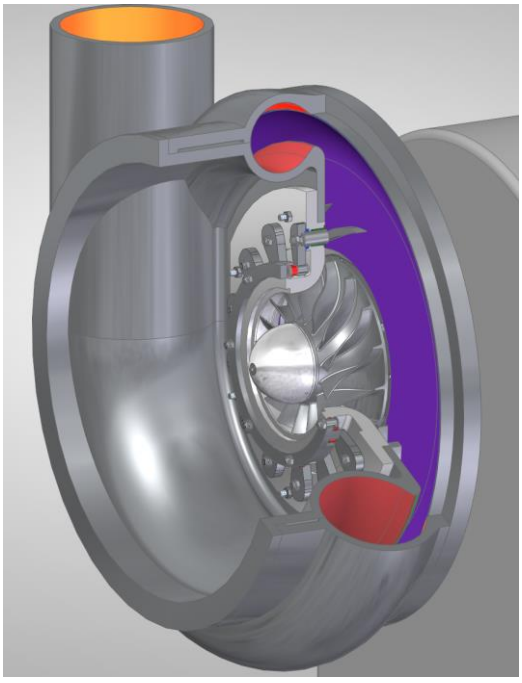

Fig. 5.4 VVD blade angle adjustment mechanism [image generated by the author]

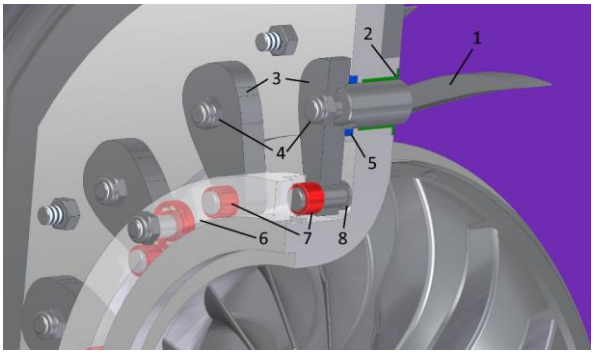

Fig. 5.5 Section through the VVD adjustment mechanism, where: 1 – VVD blade; 2 – Teflon bushing; 3 – lever; 4 – nut; 5 – sealing gasket; 6 – adjusting ring; 7 – needle roller bearings; 8 – bolt [image generated by the author]

Built to a high precision class, the mechanical components ensure minimal deviation, and the angular differences between blades can be considered insignificant.

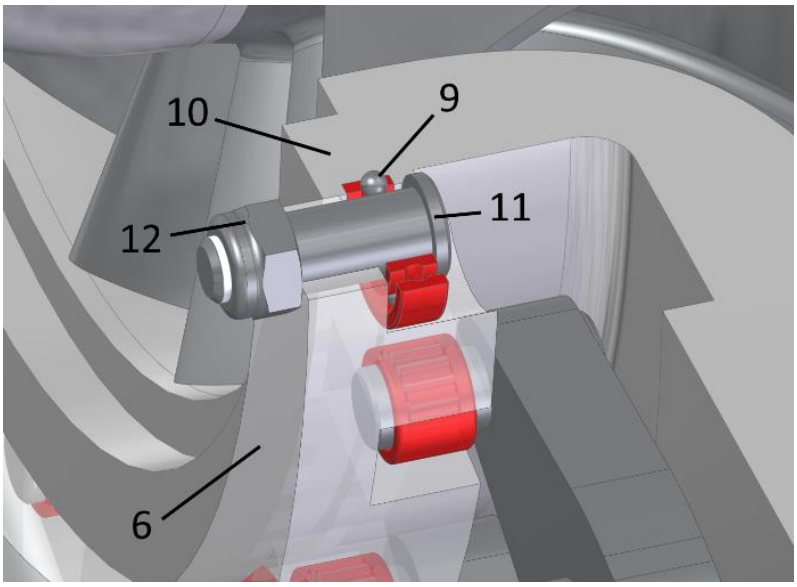

Fig. 5.6 Section through the VVD adjustment mechanism, where: 6 – adjusting ring; 9 – bearing; 10 – impeller front cover; 11 – bolt; 12 – nut [image generated by the author]

5.3. Integrated IGV and VVD angle adjustment mechanism

Once the curves illustrating the dependency of the VVD blade angles on the IGV blade angles are understood from experiments or computer simulations (CFD), an intermediate mechanism (Figure 5.7) can be developed. This mechanism ensures a direct correlation between these angles using only one control point (a single actuator).

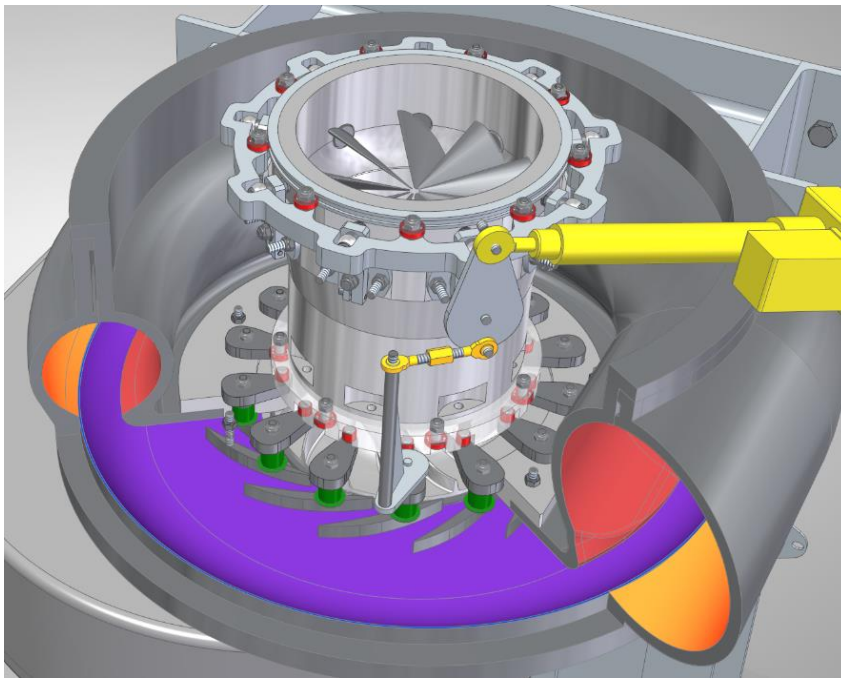

Fig. 5.7 Integrated mechanism for controlling the movements of both stators blades [image generated by the author]

The mechanism in Figure 5.7 allows for the adjustment of the VVD blade angle along with the adjustment of the IGV blade angle using a single linear actuator.

In Figure 5.8, the kinematic diagram of the mechanism is presented, enumerating its components. The operation of this system is relatively simple: when the linear actuator ***(1)*** is triggered, the IGV blade ***(3)*** undergoes a rotational movement around its own axis. The spherical joint ***(5)*** and ***(6)*** enable the continuation of this movement through a compound motion in a parallel plane. Since the cylindrical joint ***(7)*** allows rotation around only one axis, the VVD blade ***(9)*** undergoes a rotational movement around its own axis. By dimensioning the length of the IGV lever (***L_{IGV}***), the spherical joints assembly (***L_{SJ}***) and the VVD lever (***L_{VVD}***) and ignoring the effects caused by the movement of the spherical joints on the third axis (since induced errors will be below 1%), the control law of the integrated mechanism can be calculated.

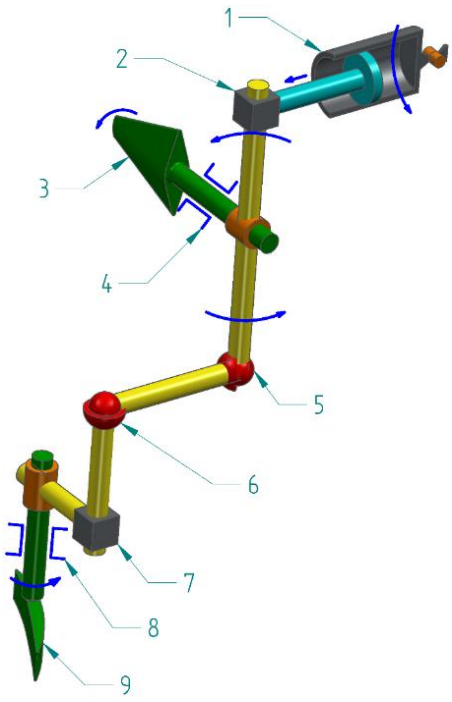

Fig. 5.8 The kinematic diagram of the mechanism, where 1 – linear actuator; 2 and 7 – cylindrical joint; 3 – IGV blade; 4 – IGV bearing; 5 and 6 – spherical joint*; 8 – VVD bearing; 9 – VVD blade [image generated by the author]*

This law defines the tilt of the VVD blades based on the tilt of the IGV blades, using formulas (5.1) – (5.4), according to [11].

The angle of rotation for the IGV blades will be set. To ensure comprehensive operational adjustment, the mechanism must allow the inlet guide vane to be adjusted from -35 degrees to +90 degrees, providing a total stroke of at least 125 degrees. Thus:

$$\measuredangle IGV = [-35°, -34°, -33°, \dots, +90°] \tag{5.1}$$

The tilt angle of the IGV blades will be:

$$\measuredangle VVD = \arcsin\left(\frac{sin(C_1)\cdot\sqrt{{L_{VVD}}^2+\left(L_{SJ}-\sqrt{{L_{SJ}}^2-2\cdot L_{IGV}\cdot L_{SJ}\cdot\cos(C_2)}\right)^2}}{L_{VVD}}\right) \tag{5.2}$$

where the terms ***C_1*** and ***C_2*** can be calculated as follows:

$$C_1 = \arcsin\left(\frac{L_{SJ}-\sqrt{{L_{SJ}}^2-2\cdot L_{IGV}\cdot L_{SJ}\cdot cos(C_2)}}{\sqrt{{L_{VVD}}^2+\left(L_{SJ}-\sqrt{{L_{SJ}}^2-2\cdot L_{IGV}\cdot L_{SJ}\cdot cos(C_2)}\right)^2}}\right) \tag{5.3}$$

$$C_2 = \arcsin\left(\frac{\sqrt{2 \cdot {L_{IGV}}^2 \cdot (1 - \cos(\measuredangle IGV)) \cdot sin\left(180 - \frac{\measuredangle IGV}{2}\right)}}{L_{SJ}}\right) - \measuredangle IGV + 90 \qquad (5.4)$$

Adjusting the parameters to L_{IGV} = 41 mm, L_{VVD} = 160 mm and L_{SJ} = 90 mm aligns the motion described by the mechanism with that shown in Figure 5.9 (green-colored points). The additional curves on the graph represent efficient adjustment curves from Figure 3.10. These curves are designed to maintain constant discharge pressure while adjusting the mass flow rate and ensuring maximum operational efficiency without the need to change the operating speed.

It can be observed that the alignment between these two curves (the motion described by the mechanism and the efficiency optimization law at the pressure ratio of 1.5) is good, with minor deviations occurring at the end of the stroke. In this case, when rotating the IGV blades to -30 degrees, the angular deviation of the VVD blades is 1.2 degrees.

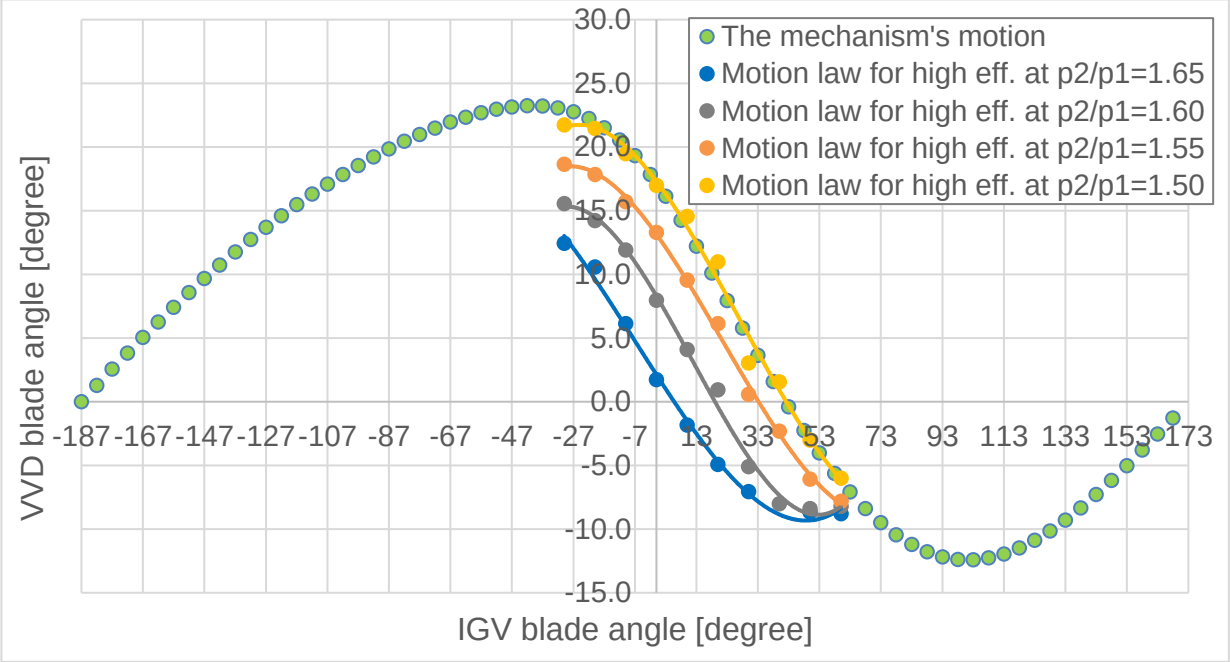

Fig. 5.9 The mechanism's motion adapted for efficient adjustment of the stators angles to achieve a pressure ratio of approximately ~1.5 [author's image]

5.4. Mock-up prototype showcasing the kinematics of stators in centrifugal blowers

As mentioned in previous chapters, centrifugal blowers are extensively used across various industries. This section features a mock-up illustrating the cross-section of the aerodynamic components of the TS6000 blower (with a nominal capacity of 6000 Nm^3/h) intended for application in wastewater treatment plants.

In Figure 5.10, the 3D model of the TS6000 mock-up is presented at a 1:2 scale. The entire mock-up is based on the actual components of the blower, modified to be physically manufacturable using additive manufacturing methods (3D printing with Fused Deposition Modeling - FDM printers).

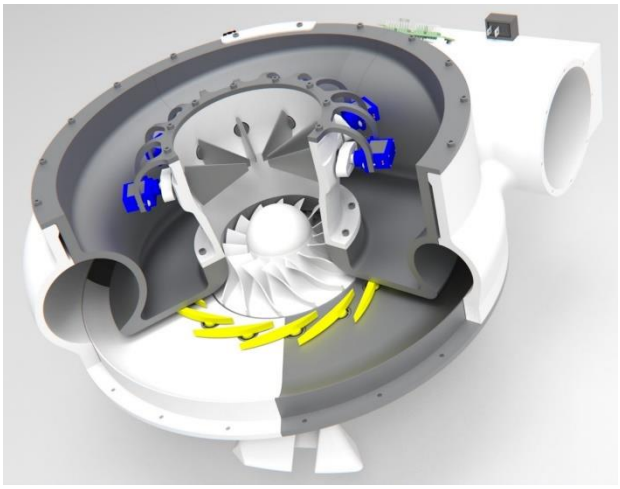

Fig. 5.10 3D model of the TS6000 blower mock-up [image generated by the author]

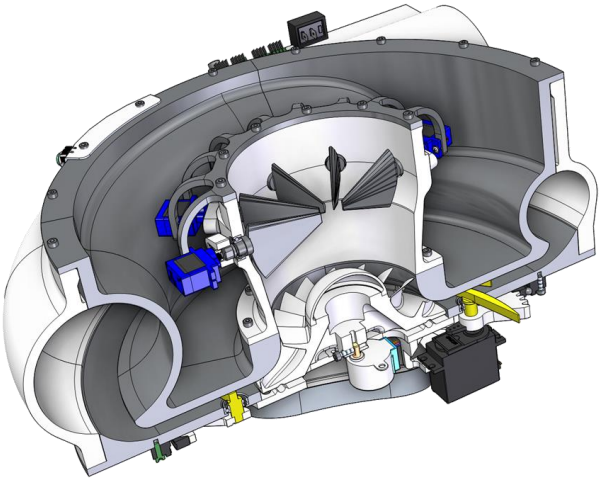

Fig. 5.11 Cross-section of the 3D mock-up model [image generated by the author]

The mock-up of the blower presented below can provide the following benefits:

- It contributes to a much better understanding of how these two stators operate during flow regulation (showing the rotational direction of the centrifugal impeller, IGV and VVD blades);
- showcases the design dimensions and overall size of all active components of the blower;
- presents a mechanical design solution for simultaneous adjustment of all blades within the VVD;
- illustrates the design solutions and adjustments to ensure the successful production of all mock-up components.

The figures 5.11 and 5.12 present cross-sections through the 3D mock-up model, showing and detailing the fastening and motion systems of the rotating components.

The volute integrated into the prototype is primarily designed to offer a view of the internal flow channel. It also integrates solutions for mounting supports, motors, batteries and electronic components.

Due to the manufacturing method (3D printing), all alignment features have been removed, so now alignment of the parts is achieved exclusively through the use of fasteners. Additionally, clearances for rotating components have been increased to eliminate the risk of frictional operation. To maintain simplicity, the motions of IGV blades is performed individually using SG90 servo motors connected to the PCA9685 module. This module enables simultaneous control and operation of all servo.

The IGV or VVD blades are mounted on 688ZZ ball bearings, guided in the flow channel by the two parallel surfaces at the shaft end.

All servos are secured to the casing through a flexible connecting element, capable of adapting to all deviations resulting from the 3D printing process.

The centrifugal impeller is attached to the main casing using the 28BYJ-48 stepper motor which receives commands through the ULN2003 driver. This configuration enables digital control over both the rotation direction and speed.

Due to the small size of the motor shaft, angular deviations can become significant during final assembly. To anticipate potential misalignment during rotation, both the impeller and the piece behind the hub disc incorporate a ball bearing track. This track compensates for any angular deviations that may occur due to uneven assembly.

The impeller cone guides the air from the center of the impeller's axis of rotation and is secured to the assembly by clamping.

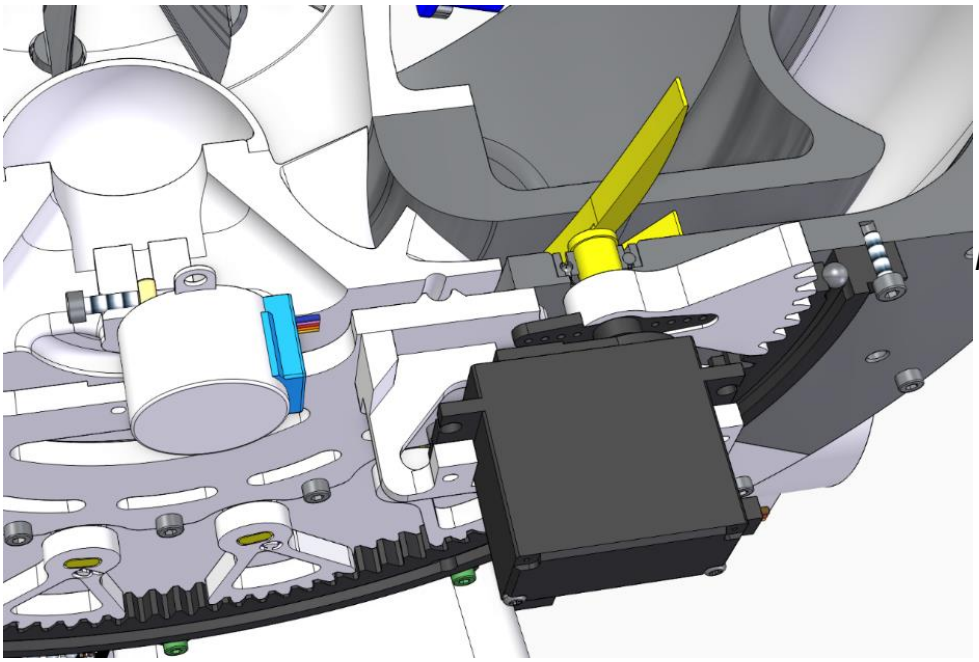

Fig. 5.12 The detail within the SPR region [image generated by the author]

The VVD blades, shown in detail in figure 5.12, are driven simultaneously by an adjustment mechanism consisting of gear sectors guided by a toothed crown. This crown has involute teeth on the inside and a track on the outside, which is also present on the connecting piece. The balls in the resulting channel ensure continuous clearance between the casing and the toothed mechanical components.

All blades are driven by a single SG5010 servo motor, which is connected to the same module used by the IGV servos. To simplify the mock-up, VVD blade supports use bearings identical to those in the IGV configuration.

Additionally, the method of securing by lightly tightening between the gear wheel sectors and the VVD blades has been addressed. Each blade is now positioned using two parallel surfaces located at the end of its shaft.

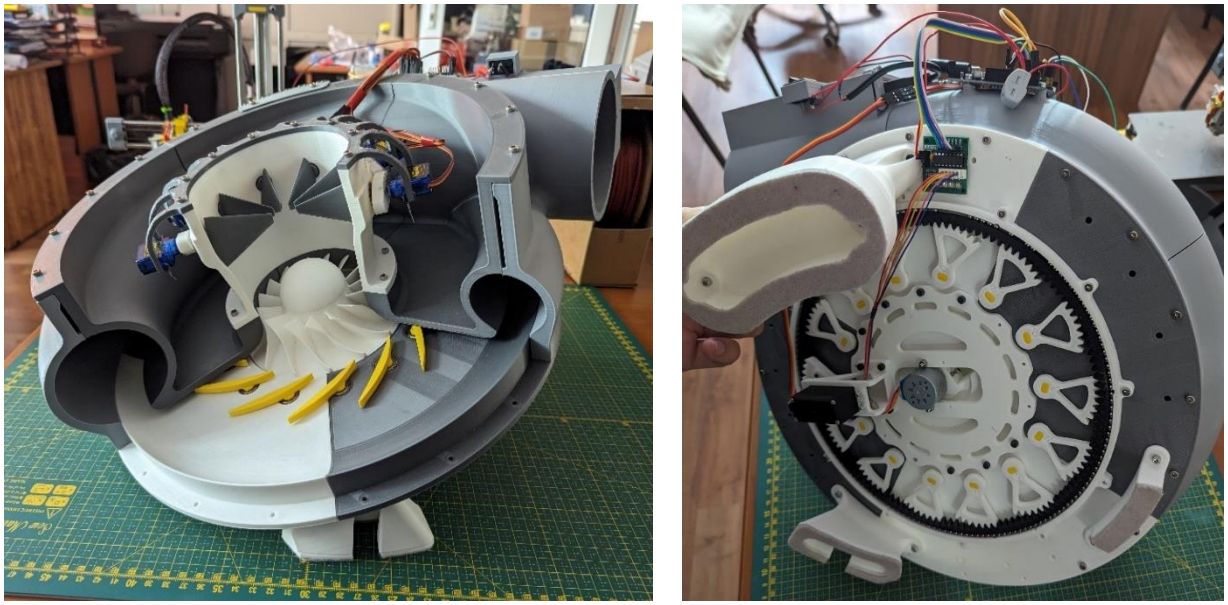

Fig. 5.13 The printed and assembled mock-up of the TS 6000 blower at a 1:2 scale [author's image]

In Figure 5.13, the functional mock-up, printed and assembled, of the TS6000 blower at a 1:2 scale is shown. Its overall dimensions are 411x386x272.

CHAPTER 6 The energetic efficiency of centrifugal blowers used in wastewater treatment plants

It is well known that centrifugal blowers used in wastewater treatment plants have the essential requirement to operate continuously for years with only brief maintenance periods allowed. Therefore, efficiency is an important factor, as it directly affects electricity bills. For instance, a slight one percent decrease in efficiency for a 100 kW centrifugal blower results in an additional consumption of at least 1 kW per hour. This translates to an inevitable energy waste of over 8760 kW per year.

In wastewater treatment plants, the required flow rate varies constantly (figures 1.4 and 1.5), determined by the oxygen sensor installed in the aeration basins. In certain geographical areas, this parameter fluctuates significantly from one season to another (for example: the required air flow in wastewater treatment plants in Constanța (Romania) can double during the summer).

Figure 6.1 compares how efficiently the single-stage blower (Figure 3.4) performs when the flow rate varies, taking into account all the efficiency curves shown in Figures 3.8 and 3.9. These curves reflect adjustments in operational parameters with stators. Adjusting the stators expands the stable operating range: the flow rate can be decreased from 0.7 kg/s to 0.4 kg/s and slightly increased from 1.822 kg/s to 1.904 kg/s at the opposite end.

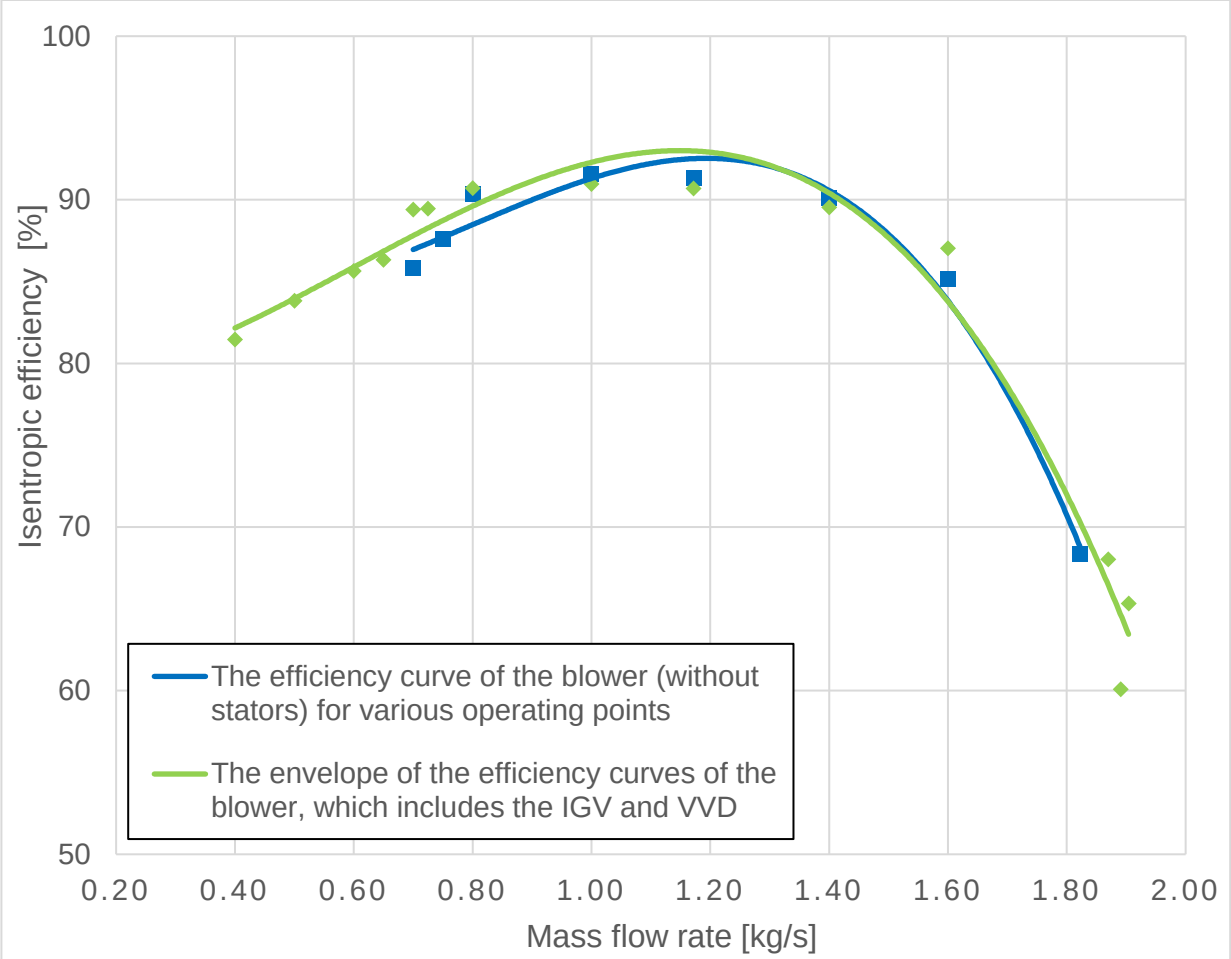

Fig. 6.1 Comparison between those two efficiency characteristic curves obtained at constant speed. [author's image]

Figure 6.1 shows that using the blower without stators results in better efficiencies at the nominal point. However, at other operating points, both the efficiency value and the stable operating range increase when adjusting the operating parameters with both stators (inlet guide vane and variable vane diffuser).

Thus, even though at the nominal operating point (1.172 kg/s), the efficiency is 0.63% higher when using the blower without stators, at lower flow rates (0.7 kg/s), the efficiency increases by 3.61% when adjusted with those two stators. Conversely, at higher flow rates (1.822 kg/s), the efficiency increase is 3.05%. Moreover, the flow adjustment range has been expanded by 25.6% for lower flow rates and by 7% for higher flow rates (compared to the nominal flow rate).

In wastewater treatment applications, flow rates must be adjusted frequently and by substantial percentages while maintaining constant discharge pressure. By using both inlet guide vane and variable vane diffuser, centrifugal blowers achieve high efficiencies across nearly all operating points while minimizing power consumption. Therefore, employing both stators remains the best and most efficient method for adjusting the mass flow rate in these applications.

General conclusions

Within the context of this doctoral thesis, the author has focused on a detailed study of high-pressure centrifugal blowers, aiming primarily to enhance the energy efficiency of existing turbomachinery by equipping them with aerodynamically profiled blades installed upstream and downstream of the impeller.

The originality of the work lies in identifying how the two stators (inlet guide vane and variable vane diffuser) correlate, ensuring effective flow adjustment to maintain higher operational efficiency, all while maintaining consistent rotational speed and discharge pressures.

The paper begins by analyzing existing articles and scientific works in the academic and scientific spheres. It then discusses various types of blowers, details the construction of centrifugal blowers and explores methods to enhance operational efficiency.

Research has shown that at flow rates lower or higher than the nominal one (the point at which separation does not occur) there is a pre-rotation either in the direction (at lower flow rates) or opposite to the direction of rotation (at higher flow rates) of the impeller, influenced by the tangential component of velocity (the angle of the relative flow β_1 changes). Adjusting the β_1 flow angle will consistently lead to separation on the pressure side of the blade profile at lower flow rates and on the suction side at higher flow rates.

To enhance energy efficiency, the incidence angle must be adjusted so that the inlet flow angle β_1 into the centrifugal impeller aligns closely or equals the geometric angle β_1 determined during manufacturing. Upon exiting the impeller, the fluid adopts the flow angle α_2, which dictates the position of the radial blades (VVD), ensuring maximum efficiency. If the VVD is not aligned with the flow direction determined by the absolute velocity angle α_2, separation may occur on both the pressure and suction sides along the aerodynamic profile, resulting in penalties in term of efficiency and head.

To elaborate on the phenomena occurring within turbomachinery, a calculation methodology was developed for designing blowers, exemplified by the design of a blower with a flow rate of 3500 Nm^3/h (1.172 kg/s) at a pressure ratio of 1.6.

Using new software and computational methods based on the Navier-Stokes flow equations, the calculated impeller has been improved and blades for both stators have been generated.

Numerical CFD simulations were also conducted using the ensemble formed by the impeller and the two types of stators (IGV and VVD), enabling the generation of characteristic curves for the centrifugal blower. It was highlighted that by employing the IGV and VVD, the stable operating range of the turbomachine has significantly expanded, while maintaining high efficiencies across the majority of operating points.

The original contributions in Chapter 3 involve obtaining the laws of variation between the two stators to efficiently control the flow rate while maintaining constant

rotational speed and discharge pressures. On the one hand, the control law adjusts with changes in discharge pressure, while on the other hand, it preserves the shape of the curve when this parameter is modified.

By comparing the results obtained from the experimental test rig presented in Chapter 4 with those from numerical simulations, all existing CFD simulations in the study were successfully validated. The discrepancies between these results were at most 2.5%.

Based on the correlation law between the IGV and VVD blades, a feasible mechanical solution for their adjustment was designed and presented. The developed mechanism can be used for both independent adjustment of each blade type and combined adjustment (the angle of the VVD blades is controlled by the position of the IGV blades).

By analyzing the efficiencies obtained throughout the study, the benefits associated with upgrading the existing blowers by adding these two stators were highlighted. Specifically, an expansion of the stable operating range by 26.6% at lower flow rates and by 7% at higher flow rate conditions was achieved. Additionally, efficiencies could increase by up to 3.61% at certain operating points.

In conclusion, this thesis makes significant contributions to the field of turbomachinery by presenting methods to enhance the energy efficiency of centrifugal blowers through the development of an integrated system for continuous flow control while maintaining quasi-constant efficiency.

Original contributions

The author of this doctoral thesis showcases the results achieved in enhancing the energy efficiency of high-pressure centrifugal blowers through the publications during the thesis preparation period [11], [12], [13].

The thesis pursues several aspects aimed at increasing efficiencies and maintaining them at high levels. Among the most significant contributions are:

1. The work starts by synthesizing the most important articles and scientific studies in the field of compressors and centrifugal blowers. This section provides a comprehensive perspective on aerodynamic components and discusses methods to improve the operational efficiencies of turbomachinery.
2. The thesis advances a calculation methodology for the preliminary design of main aerodynamic components, including the centrifugal impeller and volute. This approach enables the design of centrifugal blowers with enhanced efficiencies while providing estimations of their performance outcomes.
3. Using new design and verification methods (based on numerical flow simulations), the main elements of a centrifugal blower have been generated and improved, including the centrifugal impeller, the inlet guide vane blades and the variable vane diffuser blades. The thesis's originality lies in the extensive number of CFD simulations used to establish a mathematical correlation law between these stators

(IGV and VVD), enabling efficient flow adjustment to maximize operational efficiency while maintaining consistent discharge pressures.

4. Using numerical simulations, characteristic curves were plotted, demonstrating that the stable operating range of the simulated blower was expanded by incorporating both stators into its design.
5. A test rig for a centrifugal blower with precise flow control (incorporating both stators) was presented. Using this setup, characteristic curves and the control law for both stators were plotted to achieve maximum efficiency when adjusting the flow rate while maintaining constant discharge pressure.
6. To develop a mechanism for adjusting the angles of both stators, various mechanical systems were designed and presented. These designs enable the rotation of the IGV and VVD blades both independently (with each stator rotated separately using two distinct actuators) and in a synchronous manner (where a single actuator controls the movement of both stators simultaneously).
7. A scale 1:2 model of a centrifugal blower has been designed and fabricated using new additive manufacturing technologies (3D printing). This mock-up illustrates the functioning of turbomachinery, while also validating the selected mechanical and electronic solutions for driving the aerodynamic components.
8. A detailed analysis has been conducted highlighting the advantages of using both stators to adjust the flow rate of centrifugal blowers used for wastewater treatment plants, as opposed to other regulation methods.

Perspectives for further development

The domain of compression units, particularly centrifugal blowers and compressors, is advancing rapidly. The introduction of new computational methods and validation techniques based on CFD simulations has pushed the efficiencies of these turbomachines to exceptionally high levels, nearing their maximum possible performance.

Future perspectives focus more on designing and implementing compression units within systems where the primary goal is maximizing energy savings.

The new types of centrifugal blowers are represented by machines that no longer require speed increasers, as the centrifugal impeller is directly mounted on the shaft of high-speed permanent magnet motors. These motors provide both the necessary speed and torque, while axial and radial forces generated by the impeller's weight and its aerodynamics are handled by aerodynamic bearings integrated into the motor. This approach entirely removes the necessity for speed increasers (such as gears, oil systems, pumps, filters etc.), resulting in enhanced overall efficiency by eliminating mechanical losses caused by friction between intermediate components (between the motor and the impeller).

Published papers

ISI-indexed journal papers

1. ***Stănescu, T.***, Ușeriu, D. (2024). Performance Analysis Of Curved Shape On The Inlet Guide Vanes In Centrifugal Blowers. Aerospace Research in Bulgaria, vol. 36, doi: 10.3897/arb.v36.e13 [în curs de indexare]
2. Petrescu, V., Săvescu, C., ***Stănescu, T.***, et al. (2024). Experimental Analysis of Twin Screw Compressor's Energetic Efficiency Depending on Volume Ratio. Engineering, Technology & Applied Science Research (ETASR), vol. 14, no. 2, doi: 10.48084/etasr.6425

ISI-indexed conference papers

1. Vlăducă, I., Borzea, C., Vasile, M. L., ***Stănescu, T.***, et al. (2021). Automation Control System for Naval Propulsion Retrofitting. 2021 International Conference on Applied and Theoretical Electricity (ICATE), Craiova, Romania, pp. 1-6, doi: 10.1109/ICATE49685.2021.9465065
2. Salze, E., Gea-Aguilera, F., Buszyk, M., ***Stănescu, T.***, et al. (2024). Noise Reduction Of Aero-Engines Using Innovative Stators With Leading Edge Features. 30th AIAA/CEAS Aeroacoustics Conference [acceptat spre publicare]

IIIE-indexed conference papers

1. Isac, R., ***Stănescu, T.***, Petrescu, V. (2023). Infrared Thermography - Extending Operating Life Of Natural Gas Compression Equipment With Screw Compressor. 11th International Conference on Energy and Environment (CIEM), București, România
2. ***Stănescu, T.***, Petrescu, V., Isac, R., Presura-Chirilescu, E., et al. (2023). Performance Analysis of Centrifugal Blowers with Inlet Guide Vane Control under Different Inlet Conditions. 11th International Conference on Energy and Environment (CIEM), București, România
3. Petrescu, V., Tomescu, S., Vasile, E., ***Stănescu, T.***, et al. (2023). The Influence of Clearances on Energy Efficiency in Screw Compressors. 11th International Conference on Energy and Environment (CIEM), București, România

BDI-indexed journal papers

1. ***Stănescu, T.***, Badea, G. P., Stan, N. D., Presură-Chirilescu, E. (2019). Analysis Of The Volumetric Efficiency Of The Blower Rotors With Lobes. TURBO, vol. VI (2019), no. 2
2. ***Stănescu, T.***, Stan, N. D., Badea, G. P., Vasile, E., et al. (2020). Replacement Of Conventional Couplings With 3D Printed Couplings. TURBO, vol. VII (2020), no. 1
3. ***Stănescu, T.***, Badea, G. P., Ciobotaru, D., Ușeriu, D. (2021). Integrated Mechanism For Simultaneous Adjustment Between Inlet Guide Vanes And Diffuser Vanes. TURBO, vol. VIII (2021), no. 1
4. Vlăducă, I., Nechifor, C. V., Vasile, M. L., ***Stănescu, T.***, et al. (2022). Hydrogen Storage in Offshore Salt Caverns for Reducing Ships Carbon Dioxide Footprint. Technium, vol. 4, No. 9, pp. 1-11
5. Hank, A., Suciu, C. P., Ușeriu, D., ***Stănescu, T.***, et al. (2022). Design And Analysis Of Supersonic Turbine Rotor Blades. TURBO, vol. IX (2022), no. 1

6. Petrescu, V., ***Stănescu, T.***, Vasile, E., Isac, R., et al. (2023). Theoretical And Experimental Research On The Pressure Variation In The Compression Chamber Of The Oil Injected Screw Compressor. U.P.B. Sci. Bull., Series D, Vol. 85, Iss. 4

Patent

1. Ușeriu, D., ***Stănescu, T.*** (2023) Cap De Imprimare Echipat Cu Un Radiator Bimetalic Cu Aplicație În Imprimantele Tridimensionale Cu Depunere De Material Termoplastic. Registratura OSIM: A/0076/ 28 NOV 2023.

SELECTIVE BIBLIOGRAPHY

[1] ***Ansys, “Ansys Vista.” Accessed: Oct. 02, 2022. [Online]. Available: https://www.ansys.com/products/fluids/ansys-vista-tf

[2] ***Ansys, “Ansys Blademodeling.” Accessed: Oct. 02, 2022. [Online]. Available: https://www.ansys.com/products/fluids/ansys-blademodeler

[3] ***Cadence, “Numeca Fine Turbo.” Accessed: Oct. 02, 2022. [Online]. Available: https://www.numeca.com/product/omnis-turbo-agile

[4] ***CFD Online, “Dimensionless wall distance (y plus).” Accessed: May 23, 2024. [Online]. Available: https://www.cfd-online.com/Wiki/Dimensionless_wall_distance_(y_plus)

[5] Burger, G. *et al.*, “Modeling Aeration Performance for Energy Reduction,” *WEFTEC*, 2019.

[6] Guo, W., Z. Zuo, J. Sun, H. Hou, Q. Liang, and H. Chen, “Experimental investigation on off-design performance and adjustment strategies of the centrifugal compressor in compressed air energy storage system,” *J. Energy Storage*, vol. 38, p. 102515, 2021, doi: https://doi.org/10.1016/j.est.2021.102515.

[7] Huenteler, J., M. Yang, Y. Zhang, and T. Bamba, “Influence of the volute on the flow in a centrifugal compressor of a high-pressure ratio turbocharger,” *Proc. Inst. Mech. Eng. Part A J. Power Energy*, vol. 224, Dec. 2010, doi: 10.1243/09576509JPE968.

[8] Jenkins, T., “Calculating Aeration Flow and Pressure Requirements,” in *Bower Vacuum Best Practices*, 2016.

[9] Qingyi, S., C. Jian, and Z. Bo, “Performance prediction of centrifugal compressor based on a new volute loss model and corrected theoretical work,” *Energy Sci. Eng.*, vol. 11, no. 2, pp. 685–698, Feb. 2023, doi: https://doi.org/10.1002/ese3.1354.

[10] Rasmussen, P. and R. Kurz, “Centrifugal Compressor Applications - Upstream And Midstream.,” in *Texas A&M University. Turbomachinery Laboratories*, 2009. doi: doi.org/10.21423/R1664Q.

[11] Stănescu, T., G.-P. Badea, D. Ciobotaru, D. Ușeriu, and G.-I. Bălan, “Integrated mechanism for simultaneous adjustment between inlet guide vanes and diffuser vanes,” *Turbo*, vol. VIII, pp. 51–57, 2021.

[12] Stanescu, T., V. Petrescu, R. Isac, E. Presură-Chirilescu, D. Useriu, and G. Badea, “Performance Analysis of Centrifugal Blowers with Inlet Guide Vane Control Under Different Inlet Conditions,” in *11th International Conference on ENERGY and ENVIRONMENT (CIEM)*, Oct. 2023, pp. 1–5. doi: 10.1109/CIEM58573.2023.10349772.

[13] Stanescu, T. and D. Useriu, “PERFORMANCE ANALYSIS OF CURVED SHAPE ON THE INLET GUIDE VANES IN CENTRIFUGAL BLOWERS,” *Aerosp. Res. Bulg.*, vol. 36, pp. 147–156, Jan. 2024, doi: 10.3897/arb.v36.e13.